NASA CR-120799
UARL K910962-12

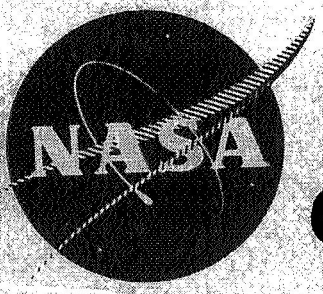

FINAL REPORT

TRANSIENT MODEL OF HYDROGEN/OXYGEN REACTOR

by
ARTHUR S. KESTEN
and
JOSEPH J. SANGIOVANNI

prepared for

NATIONAL AERONAUTICS AND SPACE ADMINISTRATION

FEBRUARY, 1971

CONTRACT NAS 3-13317

United Aircraft Research Laboratories

UNITED AIRCRAFT CORPORATION

EAST HARTFORD, CONNECTICUT 06108

NOTICE

This report was prepared as an account of Government-sponsored work. Neither the United States, nor the National Aeronautics and Space Administration (NASA), nor any person acting on behalf of NASA:

A.) Makes any warranty or representation, expressed or implied, with respect to the accuracy, completeness, or usefulness of the information contained in this report, or that the use of any information, apparatus, method, or process disclosed in this report may not infringe privately-owned rights; or

B.) Assumes any liabilities with respect to the use of, or for damages resulting from the use of, any information, apparatus, method or process disclosed in this report.

As used above, "person acting on behalf of NASA" includes any employee or contractor of NASA, or employee of such contractor, to the extent that such employee or contractor of NASA, or employee of such contractor prepares, disseminates, or provides access to any information pursuant to his employment or contract with NASA, or his employment with such contractor.

Requests for copies of this report should be referred to

National Aeronautics and Space Administration
Scientific and Technical Information Facility
P. O. Box 33
College Park, Maryland 20740

NASA CR-120799
UARL K910962-12

FINAL REPORT

TRANSIENT MODEL OF HYDROGEN/OXYGEN REACTOR

by
ARTHUR S. KESTEN
and
JOSEPH J. SANGIOVANNI

prepared for

NATIONAL AERONAUTICS AND SPACE ADMINISTRATION

FEBRUARY, 1971

CONTRACT NAS 3-13317

TECHNICAL MANAGEMENT
NASA LEWIS RESEARCH CENTER
CLEVELAND, OHIO
ADVANCED ROCKET TECHNOLOGY BRANCH
P.N. HERR

United Aircraft Research Laboratories
UNITED AIRCRAFT CORPORATION
EAST HARTFORD, CONNECTICUT 06108

Report K910962-12

Transient Model of Hydrogen/Oxygen Reactor

Final Report

January 14, 1970 - January 13, 1971

Contract NAS 3-13317

TABLE OF CONTENTS

ABSTRACT

The utility of a catalytic ignition system to promote hydrogen-oxygen combustion can be limited by the transient response of the system. The transient behavior of a reactor packed with porous catalyst particles is a function of film and pore diffusion of heat and mass as well as the chemical kinetics of the catalytic reaction. A model has been developed which permits computation of concentration and temperature profiles in the bulk gas phase and within porous catalyst particles as functions of time for given reaction rate expressions. A computer program representing this model has been used to evaluate the relative effects of various design and operating characteristics of typical reactor systems on the transient behavior of these systems.

FOREWORD

This work was performed by United Aircraft Research Laboratories for the National Aeronautics and Space Administration under Contract NAS 3-13317 initiated January 14, 1970.

Included among those who cooperated in performance of the work under Contract NAS 3-13317 were Dr. A. S. Kesten, Program Manager, Mr. J. J. Sangiovanni, Dr. W. G. Burwell, Chief, Kinetics and Thermal Sciences Section, Mrs. E. Smith, and Mr. D. B. Smith of UARL.

This work was conducted under program management of the NASA Lewis Research Center and the Technical Manager was Mr. P. N. Herr, NASA Lewis Research Center, Cleveland, Ohio.

Report K910962-12

Transient Model of Hydrogen/Oxygen Reactor

Final Report

January 14, 1970 - January 13, 1971

Contract NAS 3-13317

SUMMARY

The Research Laboratories of United Aircraft Corporation under contract with the National Aeronautics and Space Administration have performed an analytical study of the transient behavior of a hydrogen/oxygen catalytic ignition system. This final technical report summarizes work which was performed under Contract NAS 3-13317 from January 14, 1970 to January 13, 1971. Work during this period has included the development of a computer program which is used to calculate temperature and species concentration profiles as functions of time in typical reaction chamber configurations. The computer program is based upon a mathematical model of the reactor system which considers both thermal and catalytic reaction of hydrogen and oxygen, along with simultaneous heat and mass transfer between the bulk gas phase and the gas within the pores of the catalyst pellets. The possibility that water vapor produced by catalytic reaction within hot catalyst particles might condense or freeze in the colder bulk gas phase has been taken into account in the model. The computer program has been used to evaluate the relative effects of chamber pressure, feed temperature, initial bed temperature, stoichiometry, mass flow rate, and catalyst bed configuration on the transient behavior of the reactor system.

INTRODUCTION

Effective design of a catalytic ignition system to promote hydrogen-oxygen combustion requires the capability for predicting the effects of the design and operating characteristics of the reactor system on the transient and steady-state performance of the system. This general capability did not exist although the feasibility of using catalysts to promote hydrogen-oxygen combustion had been demonstrated in a number of experimental investigations (Refs. 1, 2 and 3).. These investigations did not adequately assess the effects on reactor performance of such parameters as chamber pressure, feed temperature, stoichiometry, mass flow rate, and catalyst size distribution. Nor did these investigations adequately specify ignition limits or ignition delay times. To achieve this information, a comprehensive theoretical analysis is required which considers the simultaneous processes of heat transfer, diffusion, and chemical reaction in the catalytic reactor. Such an analysis was performed at UARL in order to establish procedures capable of predicting the steady-state behavior of the system (Refs. 4 and 5). These procedures have been used to demonstrate the effects of various systems parameters on the steady-state performance of the reactor, and thus to define the regimes in which ignition is possible. Preliminary investigations at UARL indicated that the steady-state analysis could be used as a basis for the development of a transient model of the hydrogen-oxygen system.

Based upon the above investigations, a comprehensive analytical program was formulated with the objectives of (1) developing a transient analysis of a continuous flow hydrogen-oxygen catalytic ignition system to permit the prediction of temperatures, pressures, and species concentrations as functions of time as well as axial position in typical reactor systems, (2) developing a computer program based on this analysis, and (3) performing calculations using this computer program to demonstrate the effects of various system parameters on the transient performance of the reactor, and thus to define ignition delay times. This effort is described in detail in succeeding sections of this report.

DISCUSSION

Transient Model of Hydrogen-Oxygen Catalytic Ignition System

The analysis of a catalytic ignition system to promote hydrogen-oxygen combustion pertains to a reaction chamber of arbitrary cross section packed with catalyst particles into which hydrogen and oxygen are injected. Catalyst particles are represented as "equivalent" spheres with a diameter taken as a function of the particle size and shape. Both thermal and catalytic reaction of hydrogen and oxygen are considered in developing equations describing the concentration distributions of these reactants. Diffusion of reactants from the interstitial (free-gas) phase to the outside surface of the catalyst pellets is taken into account. Since the catalyst material is impregnated on the interior and exterior surfaces of porous particles, the diffusion of reactants into the porous structure must also be considered. In addition, the conduction of heat within the porous particles must be considered since the hydrogen-oxygen reaction is accompanied by the evolution of heat. The possibility that water vapor produced by catalytic reaction within hot catalyst particles might condense or freeze in the colder bulk gas is also taken into account in the model.

The model permits the computation of concentration and temperature distributions in the bulk gas phase and within the catalyst particles as functions of time for a given reaction rate expression. Thus, the temporary reduction in catalytic activity caused by capillary condensation or freezing of the reaction product in cold catalyst particles can be accommodated once the effect of condensation on activity has been determined. Models are suggested to describe the effect of condensation on reaction rate; evaluation of these models requires comparison of results obtained using the models in the detailed transient reactor analysis with experimental results obtained from reactor tests. Unfortunately, as noted in the subsequent section on "Kinetics Information" consistent experimental data has not become available as of the end of the contract period.

The general equations describing the rates of change of enthalpy and species concentrations with time and axial distance in the interstitial phase can be simplified by noting that gas velocities are sufficiently high so that the time lag from the reactor inlet to any axial position for the gas is negligible compared with other transient effects. These equations can then be written as

$$\frac{\partial (W_{O_2})_i}{\partial Z} = - \frac{1}{G} \left\{ r_{hom}\, \delta + (k_c)_{O_2}\, A_p \left[(\rho_{O_2})_i - (\rho_{O_2})_{ps} \right] \right\} \tag{1}$$

$$\frac{\partial (W_{H_2})_i}{\partial Z} = - \frac{1}{G} \left\{ r_{hom}\, \delta \frac{2M_{H_2}}{M_{O_2}} + (k_c)_{H_2}\, A_p \left[(\rho_{H_2})_i - (\rho_{H_2})_{ps} \right] \right\} \tag{2}$$

$$\frac{\partial (W_{H_2O})_i}{\partial Z} = \frac{1}{G}\left\{ r_{hom}\,\delta\,\frac{2M_{H_2O}}{M_{O_2}} - (k_c)^{(v)}_{H_2O}\; A_p\left[(\rho_{H_2O})^{(v)}_i - (\rho_{H_2O})^{(v)}_{ps} \right] \right\} \tag{3}$$

The partial derivatives of species concentrations with respect to axial distance are then given by

$$\frac{\partial (\rho_J)_i}{\partial Z} = \rho_i \frac{\partial (W_J)_i}{\partial Z} + (W_J)_i \frac{\partial \rho_i}{\partial Z} \tag{4}$$

where

$$\frac{1}{\rho_i}\frac{\partial \rho_i}{\partial Z}\left[1-(W_{H_2O})^{(s)}_i - (W_{H_2O})^{(\ell)}_i \right] = \frac{\partial (W_{H_2O})^{(s)}_i}{\partial Z} + \frac{\partial (W_{H_2O})^{(\ell)}_i}{\partial Z}$$

$$+\frac{\rho_i^{(V)}}{\rho_i}\left[\frac{1}{P}\frac{\partial P}{\partial Z} + \frac{1}{\overline{M}^{(v)}}\;\frac{\partial \overline{M}^{(v)}}{\partial Z} - \frac{1}{T_i}\;\frac{\partial T_i}{\partial Z} \right] \tag{5}$$

and

$$\frac{1}{\overline{M}^{(v)}}\;\frac{\partial \overline{M}^{(v)}}{\partial Z} = -\left[\frac{\sum\limits_{J\,(vapor)} \frac{\partial (W_J)_i}{\partial Z} \Big/ M_J}{\sum\limits_{J\,(vapor)} \frac{(W_J)_i}{M_J}} \right] \tag{6}$$

Heat and mass transfer coefficients may be estimated from (Ref. 6)

$$h_c = 0.61\,\overline{C}_f^{(v)}\,G\left(\frac{\overline{C}_f^{(v)}\,\mu}{K} \right)^{-0.667}\left(\frac{G}{A_p \mu} \right)^{-0.41} \tag{7}$$

$$(k_c)_J = \frac{0.61 G}{\rho^{(v)}}\left(\frac{\mu}{\rho_i^{(v)} (D_i)_J} \right)^{-0.667}\left(\frac{G}{A_p \mu} \right)^{-0.41} \tag{8}$$

In the entrance region of the reactor, where the temperature in the interstitial phase is low enough to cause freezing of the water vapor diffusing out of the catalyst particles, the enthalpy of the interstitial phase varies as

$$\frac{\partial h_i}{\partial Z} = -\frac{1}{G}\left\{ H_{O_2}\, r_{hom}\,\delta + h_c\, A_p\left[T_i - (T_p)_s \right] + \frac{4 h_w}{d_c}\left[T_i - T_w \right] \right.$$

$$\left. + (k_c)^{(v)}_{H_2O}\; A_p\left[(\rho_{H_2O})^{(v)}_i - (\rho_{H_2O})^{(v)}_{ps} \right]\left[\Delta H^f + \Delta H^c \right] \right\} \tag{9}$$

where the term involving h_w in Eq. (9) represents the heat loss from the bulk vapor to the wall of the reactor. Taking the reactor wall temperature as uniform, the rate of change of wall temperature with time is

$$m_w C_w \frac{dT_w}{dt} = \pi d_c \int_0^L h_w (T_i - T_w)\, dz - h_a A_w (T_w - T_a) \tag{10}$$

where the last term on the right side of Eq. (10) represents the heat loss by forced convection from the reactor to the surrounding atmosphere. Heat loss by natural convection or radiation can be represented in Eq. (10) by adding a term of the form $h_a' A_w (T_w - T_a)^{1.25}$ or $h_a'' A_w (T_w^4 - T_a^4)$, respectively.

In this "ice region"

$$\frac{\partial (W_{H_2O})_i}{\partial Z} = \frac{\partial (W_{H_2O})_i^{(s)}}{\partial Z} \tag{11}$$

In the higher temperature, "ice-liquid region" of the reactor, the enthalpy of the interstitial phase varies as

$$\frac{\partial h_i}{\partial Z} = \frac{1}{G} \left\{ H_{O_2} r_{hom}\, \delta + h_c A_p \left[T_i - (T_p)_s \right] + \frac{4 h_w}{d_c} \left[T_i - T_w \right] + (K_c)_{H_2O}^{(v)} A_p \left[(\rho_{H_2O})_i^{(v)} - (\rho_{H_2O})_{ps}^{(v)} \right] \left[\Delta H^c + \Delta H^f \left(\frac{h_i - h_i^{(s)}}{h_i^{(s-\ell)} - h_i^{(s)}} \right) \right] \right\} \tag{12}$$

and the rates of change of ice and liquid weight-fractions are given by

$$\frac{\partial (W_{H_2O})_i^{(s)}}{\partial z} = \frac{\partial (W_{H_2O})_i}{\partial z} \left[\frac{h_i^{(s-\ell)} - h_i}{h_i^{(s-\ell)} - h_i^{(s)}} \right] + \frac{1}{(h_i^{(s-\ell)} - h_i^{(s)})} \frac{\partial h_i}{\partial z} \tag{13}$$

$$\frac{\partial (W_{H_2O})_i^{(\ell)}}{\partial z} = \frac{\partial (W_{H_2O})_i}{\partial z} \left[\frac{h_i - h_i^{(s)}}{h_i^{(s-\ell)} - h_i^{(s)}} \right] + \frac{1}{(h_i^{(s-\ell)} - h_i^{(s)})} \frac{\partial h_i}{\partial z} \tag{14}$$

where, at a fixed axial position, z, in the ice-liquid region, the enthalpy required for melting the ice existing at that position may be calculated from

$$h_i^{(s-\ell)} = h_i(z) + \Delta H^f (W_{H_2O})_i^{(s)}(z) \tag{15}$$

At still higher temperatures, where water exists in liquid form in the interstitial phase, the change in enthalpy with distance is given by

$$\frac{\partial h_i}{\partial z} = -\frac{1}{G}\left\{H_{O_2} r_{hom}\,\delta + h_c A_p\left[T_i - (T_p)_s\right] + \frac{4h_w}{d_c}\left[T_i - T_w\right] + (k_c)^{(v)}_{H_2O} A_p\left[(\rho_{H_2O})^{(v)}_i - (\rho_{H_2O})^{(v)}_{ps}\right]\left[\Delta H^c\right]\right\} \tag{16}$$

In this "liquid region"

$$\frac{\partial (W_{H_2O})_i}{\partial z} = \frac{\partial (W_{H_2O})^{(\ell)}_i}{\partial z} \tag{17}$$

In the "liquid-vapor region" of the reactor, the enthalpy varies as

$$\frac{\partial h_i}{\partial z} = -\frac{1}{G}\left\{H'_{O_2} r_{hom}\,\delta + h_c A_p\left[T_i - (T_p)_s\right] + \frac{4h_w}{dc}\left[T_i - T_w\right] + (k_c)^{(v)}_{H_2O} A_p\left[(\rho_{H_2O})^{(v)}_i - (\rho_{H_2O})^{(v)}_{ps}\right]\left[\Delta H^c\left(\frac{h_i - h_i^{(\ell)}}{h_i^{(\ell-v)} - h_i^{(\ell)}}\right)\right]\right\} \tag{18}$$

and the rates of change of liquid and water vapor weight-fractions are given by

$$\frac{\partial (W_{H_2O})^{(\ell)}_i}{\partial z} = \frac{\partial (W_{H_2O})_i}{\partial z}\left[\frac{h_i^{(\ell-v)} - h_i}{h_i^{(\ell-v)} - h_i^{(\ell)}}\right] - \frac{1}{h_i^{(\ell-v)} - h_i^{(\ell)}}\frac{\partial h_i}{\partial z} \tag{19}$$

$$\frac{\partial (W_{H_2O})^{(v)}_i}{\partial z} = \frac{\partial (W_{H_2O})_i}{\partial z}\left[\frac{h_i - h_i^{(\ell)}}{h_i^{(\ell-v)} - h_i^{(\ell)}}\right] + \frac{1}{h_i^{(\ell-v)} - h_i^{(\ell)}}\frac{\partial h_i}{\partial z} \tag{20}$$

where, at a fixed axial position in this region, the enthalpy required for vaporizing the liquid existing at that position may be calculated from

$$h_i^{(\ell-v)} = h_i(z) + \Delta H^c (W_{H_2O})^{(\ell)}_i(z) \tag{21}$$

In the high temperature, all vapor, region of the reactor, the change in enthalpy with distance is given by

$$\frac{\partial h_i}{\partial z} = -\frac{1}{G}\left\{H'_{O_2} r_{hom}\,\delta + h_c A_p\left[T_i - (T_p)_s\right] + \frac{4h_w}{dc}\left[T_i - T_w\right]\right\} \tag{22}$$

and

$$\frac{\partial (W_{H_2O})_i}{\partial z} = \frac{\partial (W_{H_2O})^{(v)}_i}{\partial z} \tag{23}$$

Species concentrations and temperatures at the outside surfaces of the catalyst particles can be determined, together with the concentration and temperature profiles throughout the particles, using an integral equation method described in Appendix I. At some time, t, the concentrations and temperature at position x within a porous catalyst particle are given by

$$\rho_{O_2}^{*}(x,t) = -\frac{1}{4\pi D_{O_2}}\int_0^a x_0^2 \left\{ \left[\frac{r_{O_2}'(x_0,t) - r_{O_2}'(x_0,0)}{t}\right]\int_0^t t_0 G_{O_2}(x,t/x_0,t_0)\,dt_0 + r_{O_2}'(x_0,0)\int_0^t G_{O_2}(x,t/x_0,t_0)\,dt_0 - \rho_{O_2}^{*}(x_0,0)\,G_{O_2}(x,t/x_0,0)\right\} dx_0 \tag{24}$$

$$\rho_{H_2}^{*}(x,t) = -\frac{1}{4\pi D_{H_2}}\int_0^a x_0^2 \left\{ \frac{2M_{H_2}}{M_{O_2}}\left[\frac{r_{O_2}'(x_0,t) - r_{O_2}'(x_0,0)}{t}\right]\int_0^t t_0 G_{H_2}(x,t/x_0,t_0)\,dt_0 + \frac{2M_{H_2}}{M_{O_2}}\,r_{O_2}'(x_0,0)\int_0^t G_{H_2}(x,t/x_0,t_0)\,dt_0 - \rho_{H_2}^{*}(x_0,0)\,G_{H_2}(x,t/x_0,0)\right\} dx_0 \tag{25}$$

$$\rho_{H_2O}^{*}(x,t) = \frac{1}{4\pi D_{H_2O}}\int_0^a x_0^2 \left\{ \frac{2M_{H_2O}}{M_{O_2}}\left[\frac{r_{O_2}'(x_0,t) - r_{O_2}'(x_0,0)}{t}\right]\int_0^t t_0 G_{H_2O}(x,t/x_0,t_0)\,dt_0 + \frac{2M_{H_2O}}{M_{O_2}}\,r_{O_2}'(x_0,0)\int_0^t G_{H_2O}(x,t/x_0,t_0)\,dt_0 + \rho_{H_2O}^{*}(x_0,0)\,G_{H_2O}(x,t/x_0,0)\right\} dx_0 \tag{26}$$

$$T^{*}(x,t) = -\frac{1}{4\pi\kappa}\int_0^a x_0^2 \left\{ \frac{H_{O_2}'\,\kappa}{K_p}\left[\frac{r_{O_2}'(x_0,t) - r_{O_2}'(x_0,0)}{t}\right]\int_0^t t_0 G_T(x,t/x_0,t_0)\,dt_0 + \frac{H_{O_2}'\,\kappa}{k_p}\,r_{O_2}'(x_0,0)\int_0^t G_T(x,t/x_0,t_0)\,dt_0 - T^{*}(x_0,0)\,G_T(x,t/x_0,0)\right\} dx_0 \tag{27}$$

The Green's functions associated with Eqs. (24) through (27) are given by

$$G_I(x,t/x_o,t_o) = \frac{8\pi\alpha_I}{a x x_o} \sum_{n=1}^{\infty} \frac{N_n^2+(\phi_I a-1)^2}{N_n^2+\phi_I a(\phi_I a-1)} \sin\left(N_n \frac{x}{a}\right) \sin\left(N_n \frac{x_o}{a}\right) e^{-\left(\frac{N_n}{a}\right)^2 \alpha_I (t-t_o)} \qquad (28)$$

where I = O_2, H_2, H_2O or T, and N_n's are the positive roots of the characteristic equation,

$$N_n \cot N_n + (\phi_I a - 1) = 0$$

α_I and ϕ_I are the appropriate diffusion constants expressed as follows:

For mass transfer (Eqs. 24-26) $\alpha_I = D_I$ and $\phi_I = \frac{(k_c)_I}{D_I}$

For heat transfer (Eq. 27) $\alpha_I = \kappa$ and $\phi_I = \frac{h_c}{k_p}$

Equations (24) through (27) are implicit integral equations which can be solved numerically to determine the temperature and species concentrations at any point in a porous particle at any time in terms of the temperature and concentrations in the bulk gas. Since the reaction rate for this hydrogen-oxygen system is a function of oxygen concentration and temperature (see section on "Kinetics Information"), it is necessary to solve Eqs. (24) and (27) simultaneously. Numerical procedures have been developed to accomplish this and these have been programmed for digital computation. The procedures consist basically of (1) assuming the reaction rate distribution, $r'_{O_2}(x_o,t)$, at the end of a short time interval t (see Appendix I), (2) computing the concentration distributions at time t for oxygen using Eq. (24), (3) computing the temperature distribution at time t using Eq.(27), (4) computing the reaction rate, $r'_{O_2}(x_o,t)$, using the computed distributions from (2) and (3) above, and (5) comparing the computed and assumed reaction rate distributions and repeating the procedure until a desired accuracy is obtained. An iterative procedure has been developed which averages assumed and computed distributions for rate of reaction to effect rapid convergence over a fairly wide range of variables. The concentration distributions for hydrogen and water, which are not involved in the rate of reaction expression, are computed only after the rate of reaction at time t has been determined from the iterative procedure.

Kinetics Information

As noted in Ref. 4, estimating the chemical kinetic rate law and constants appropriate to the catalytic reaction of hydrogen and oxygen is quite difficult. Although a substantial number of experimental investigations have been conducted with this objective, the results of various investigators differ considerably for diverse conditions of concentration, temperature and catalyst. These results indicate that, even for low temperature reaction on platinum family metals, the reaction mechanism changes with gas composition. Reaction of chemisorbed oxygen with hydrogen molecules in the gas phase appears to be the rate-controlling step in systems where excess oxygen is present, while this relatively slow reaction does not seem to influence the overall reaction rate in systems containing excess hydrogen. For low temperature, hydrogen-rich systems, Miller and Deans (Ref. 7) and Maymo and Smith (Ref. 8) report an activation energy of approximately 5.5 kcal and an order of reaction with respect to oxygen of 0.8. In the latter study, the rate of reaction was found to be uninfluenced by the presence of water in the vapor phase. No work was done in these studies to estimate the order of reaction with respect to hydrogen. In the present work the results of Refs. 7 and 8 were used to get a reaction rate expression of the form:

$$r'_{O_2} = \alpha(\rho_{H_2})^n (\rho_{O_2})^{0.8} e^{-5000/T} \text{ lbs } O_2 \text{ reacted/ft}^3\text{-sec} \qquad (29)$$

where T is in deg R. The rate constant, α, is specific to the type and structure of the platinum family metal employed.

It was originally intended to estimate n and α for the Shell 405 catalyst by using the steady-state program (Ref. 4) to find the values of these rate constants for which calculated axial temperature profiles exhibited the best agreement with temperatures measured in engine tests reported in Ref. 9. Unfortunately, the measured temperatures reported in Ref. 9 exhibited both large radial variations and values which were higher than possible for uniformly mixed streams with the mixture ratios and inlet temperatures reported. While the indicated lack of radial mixing in the experiments make the measured temperatures of questionable value, it was feasible to use the computer program to find the values of the rate constants for which ignition or lack of ignition in the engine tests is predicted for all cases, particularly those in which ignition was marginal. These include low feed temperature or mixture ratio tests as well as tests in which the mass flow rate was particularly high. The criterion for ignition was determined by noting that when the steady-state temperature of the particles at the inlet of the bed is too low to permit water to exist in vapor form, condensation or freezing of water within the particles would ultimately render the entire bed ineffective.

Computer runs were made with various pre-exponential constants, α, using orders of reaction with respect to hydrogen, n, between zero and one in an attempt to match the ignition behavior noted in Ref. 9. Values of 3×10^7 for α and zero for n permitted the prediction of the same ignition characteristics observed in all of the

engine tests. Results of calculations made using these rate constants are shown below for cases where ignition was marginal.

Ref 9 Case No.	Upstream Chamber Pressure psia	Mass Flow Rate lb/ft^2-sec	Mixture Ratio lbs O_2/ lb H_2	Propellant Feed Temperature deg R	Ignition ? Observed	Predicted
823	13.1	0.26	0.759	237	Yes	Yes
824	15.0	0.64	0.807	225	Yes	Yes
847	14.1	0.40	0.628	235	Yes	Yes
848	10.8	0.48	0.498	210	No	No
864	15.7	1.28	0.610	235	No	No
866	90.7	3.20	0.792	235	Yes	Yes
867	57.6	3.07	0.707	210	No	No
868	81.6	5.38	0.777	210	No	No
869	42.5	2.90	0.867	260	No	No
886	112.1	3.58	0.998	235	Yes	Yes
890	125.6	3.89	1.010	310	Yes	Yes
891	53.3	3.56	0.742	210	No	No
892	124.8	3.52	0.994	280	Yes	Yes
961	98.8	5.17	1.038	210	Yes	Yes

While the effects of propellant feed temperature and mixture ratio on reactor behavior are evident, it is interesting to note the effects of mass flow rate. High mass flow rates result in high heat transfer coefficients and correspondingly low differences between particle and gas temperatures in low temperature regions where the rate of reaction is not strongly influenced by the rate of mass transfer from the gas to the surface of the particle. For a low propellant temperature, then, it is more likely for water produced by reaction in the catalyst particles to condense or freeze when the mass flow rate is high than when it is low. The behavior of Ref. 9 case 847 as opposed to case 864 exemplifies this behavior.

It is clear that in the early stages of transient operation of a catalyst bed which is initially at a low temperature, consideration should be given to the effects on transient reactor behavior of the temporary reduction in catalyst activity caused by capillary condensation or freezing of water in cold catalyst particles. Unfortunately the mechanism of catalyst "poisoning" by condensed or frozen water is open to question. While significant quantities of water could block enough pores to isolate large segments of a porous particle from the reactants, the interconnected nature of the pores and the limited time available for condensation in the hydrogen-oxygen system make it appear likely that any significant reduction in activity would be due to local condensation or freezing. A simple, reasonably general model representing this type of poisoning is given by

$$r'_{O_2}(x,t) = \left[r'_{O_2}(x,t)\right]_{NC} \left\{ \frac{1}{1+\beta\left[\rho_{H_2O}\ (x,t)\right]_c^{\gamma}} \right\} \qquad (30)$$

where $\left[r'_{O_2}(x,\ t)\right]_{NC}$ is the value the local reaction rate would assume if there were no condensed phase, and β and γ are constants to be determined by using Eq. (30) in the transient program to find the values of these constants for which calculated temperature variations with time exhibited the best agreement with temperature profiles measured in reactor experiments. The rate of buildup of local condensate (or ice) concentration with time, at temperatures low enough to permit condensation (or freezing), would be directly proportional to the local reaction rate.

Results of Calculations

Sample calculations have been made using the transient computer program to test the effectiveness of the transient model neglecting the effects of condensation or freezing of water within cold catalyst particles on catalytic reaction rates. The computed results can presently be used to evaluate the relative effects of various design and operating characteristics of the reactor system on the transient behavior of the system. One series of calculations pertains to a reactor 0.24 in. (0.006 m) long and 0.43 in. (0.011 m) in diameter packed with Shell 405 catalyst particles and run at a nominal chamber pressure of 300 psia (2.07×10^6 N/m^2). A reference case was chosen in which the initial bed temperature and the feed temperature were taken as 360 deg R (200 deg K), the mixture ratio as 1 lb O_2/lb H_2, the mass flow rate as 1.05 lb/ft^2-sec (5.1 kg/m^2-sec), and the catalyst particle size as 14-18 mesh. The calculated axial gas temperature profiles for this reference case are shown at various times following reactor startup in Fig. 1. The corresponding axial profiles of catalyst particle surface temperatures are plotted in Fig. 2. Temperature response rates are far more rapid in the upstream end of the bed where oxygen concentrations and catalytic reaction rates are high. Most of the heat transferred to the gas in the upstream section is transferred back to the particles downstream. Gas and particle surface temperatures are cross-plotted as functions of time in Fig. 3 for two axial positions, one at the end of the bed and one at approximately the midpoint of the bed. It is clear that the exit gas temperature for this case would have risen far more rapidly if the bed were half as long. In Fig. 3 temperatures are plotted from reactor startup through an arbitrary shutdown point represented by a step change in the feed mixture ratio from one to zero (i.e., subsequent to shutdown pure hydrogen is taken to flow through the reactor at the total mass flow rate). Also included in Fig. 3 is a plot of the chamber wall temperature variation with time. The relatively slow response rate is due mainly to the limited surface area available for heat transfer to the wall. Transient axial profiles of mole fraction of oxygen in the gas phase for this reference case are plotted in Fig. 4. Changes in phase of the reaction product, water, within the reactor are reflected in the oxygen concentration profiles. A shift in the profiles with time towards the upstream end of the reactor, as temperatures rise, is also evident.

In Figs. 5 and 6, transient axial gas temperature profiles are plotted for mixture ratios of 2 and 4 respectively with all other conditions taken as those of the reference case. The very dramatic effect of mixture ratio on transient response may be noted by comparing Figs. 1, 5, and 6. The effect on gas temperature at a given axial position in the reactor is far less apparent, particularly in the downstream section of the reactor where, after a short time, there is little oxygen left to react and the catalyst particles become little more than a heat sink. The variations of both exit and mid-bed gas temperatures with time are plotted in Figs. 7 and 8 respectively for the three mixture ratios.

In Fig. 9 transient axial gas temperature profiles are plotted for a feed temperature and initial bed temperature of 530 deg R (295 deg K) with all other conditions taken as those of the reference case. Similar plots are presented in Figs. 10, 11, and 12 for temperatures of 420, 330, and 300 deg R (233, 183, and 167 deg K) respectively. The effect of the combination of feed temperature and initial bed temperature on transient response is quite evident in Fig. 13 where variations in exit gas temperatures with time are compared for the five different feed temperatures.

Transient axial gas temperature profiles are plotted in Fig. 14 for an initial bed temperature of 530 deg R (295 deg K) with all other conditions, including feed temperature, taken as those of the reference case. Variations in exit gas temperature with time are compared with those of the reference case in Fig. 15.

Figures 16 and 17 illustrate the effects of doubling the mass flow rate over that of the reference case on the gas temperature transient response. Flow rate has little effect on the rates of temperature rise at early times when temperatures are low; here overall reaction rates are controlled by the rates of reaction on the catalyst surfaces. As temperatures rise the overall reaction rates are controlled by the rates of heat and mass transfer between the flowing gas and the catalyst particles; these transport processes are quite sensitive to mass flow rate as exemplified in Fig. 17.

The effects of decreasing the catalyst particle size to 25-30 mesh on temperature response rates are illustrated in Figs. 18 and 19. Heat and mass transfer rates, which vary inversely with particle size, cause temperatures to rise faster in the upstream section of the reactor and to fall faster downstream for the smaller particle size. This effect is clearly shown in Fig. 19 where gas temperatures are plotted as functions of time at two axial positions for the two particle sizes. Transient response of exit gas temperature would have been enhanced in this case if the catalytic reactor were packed with small particles upstream and larger particles downstream.

A second series of calculations was made for a reactor 0.24 in. (0.006 m) long and 0.87 in. (0.022 m) in diameter again packed with Shell 405 catalyst particles but now run at a low nominal chamber pressure of 15 psia (1.04×10^5 N/m^2). A reference case was chosen in which the initial bed temperature, feed temperature,

mixture ratio, and catalyst particle size were taken as the same as the previous reference case and the mass flow rate was taken as 0.26 lb/ft^2-sec (1.25 kg/m^2-sec). The calculated axial gas temperature profiles for this reference case are shown in Fig. 20 at various times between reactor startup and shutdown. The corresponding axial profiles of catalyst particle surface temperatures are plotted in Fig. 21. Gas and particle surface temperatures are cross-plotted as functions of time in Fig. 22 for two axial positions under both normal operating conditions and shutdown conditions. Transient axial profiles of mole fraction of oxygen in the gas phase are plotted in Fig. 23.

In Fig. 24 transient axial gas temperature profiles are plotted for a mixture ratio of 4 with all other conditions taken as those of the reference case. Variations of exit gas temperatures with time are compared for this case and the reference case in Fig. 25.

In Fig. 26 transient axial gas temperature profiles are plotted for a feed temperature and initial bed temperature of 530 deg R (295 deg K) with all other conditions taken as those of the reference case. The effect of the combination of feed temperature and initial bed temperature on transient response is shown in Fig. 27 where the transient temperature response for this case is compared with the reference case.

Finally, the effects of doubling the mass flow rate over that of the reference case on gas temperature transient response is shown in Figs. 28 and 29.

REFERENCES

1. Roberts, R. W., H. L. Burge and M. Ladacki: Investigation of Catalytic Ignition of Oxygen/Hydrogen Systems. NASA CR-54657, December 1965.

2. Development of Hydrogen-Oxygen Catalysts. NASA CR-72118, July 1966.

3. Rodewald, N., G. Falkenstein, P. Herr, and E. Prono: Evaluation and Demonstration of the Use of Cryogenic Propellants (O_2/H_2) for Reaction Control Systems, Volume II--Experimental Evaluations and Demonstration. NASA CR-72244, June 1968.

4. Kesten, A. S.: Study of Catalytic Reactors for Hydrogen-Oxygen Ignition. NASA CR-72567, July 1969.

5. Kesten, A. S.: Analytical Study of the Steady-State Behavior of a Hydrogen-Oxygen Catalytic Ignition System. Proceedings of the 12th Liquid Propulsion Meeting, Las Vegas, Nevada, November 1970.

6. Bird, R. B., W. E. Stewart, and E. N. Lightfoot: Transport Phenomena. John Wiley & Sons, Inc., New York, 1960.

7. Miller, F. W. and H. A. Deans: An Experimental Study of Nonisothermal Effectiveness Factors in Porous Catalyst. AIChE Journal, Vol. 13, 1967, pp. 45-51.

8. Maymo, J. A. and J. M. Smith: Catalytic Oxidation of Hydrogen-Intrapellet Heat and Mass Transfer. AIChE Journal, Vol. 12, 1966, pp. 845-854.

9. Investigation of Thrustors for Cryogenic Reaction Control Systems. TRW Systems Final Report, NASA Contract NAS 3-11227, March 1970.

10. Morse, P. M. and H. Feshbach: Methods of Theoretical Physics. McGraw-Hill Book Co., Inc., New York, 1953, Part I.

11. Kesten, A. S.: An Integral Equation Method for Evaluating the Effects of Film and Pore Diffusion of Heat and Mass on Reaction Rates in Porous Catalyst Particles. AIChE Journal, Vol. 15, January 1969.

12. Sangiovanni, J. J. and A. S. Kesten: Analysis of Gas Pressure Buildup Within a Porous Catalyst Particle Which is Wet by a Liquid Reactant. Chemical Engineering Science, In press.

LIST OF SYMBOLS

a	Radius of porous catalyst particle, ft(m), or, moles of species A
A	Symbol for primary reactant species A, or, surface area, $ft^2(m^2)$
A_p	Total external surface of catalyst particle per unit volume of bed, $ft^{-1}(m^{-1})$
b	Moles of species B
B	Symbol for reactant species B
C	Specific heat, Btu/lb-deg R (Cal/kg-deg K)
C_f	Specific heat of fluid in the interstitial phase, Btu/lb-deg R (Cal/kg-deg K)
$\overline{C}_f$	Average specific heat of fluid in the interstitial phase, Btu/lb-deg R (Cal/kg-deg K)
d_c	Diameter of reaction chamber, ft(m)
D	Effective diffusion coefficient in the porous catalyst particle, ft^2/sec (m^2/sec)
D_i	Diffusion coefficient of reactant gas in the interstitial phase, ft^2/sec (m^2/sec)
F	General function
G	Green's function, 1/ft-sec (1/m-sec), or, Mass flow rate, lb/ft^2-sec $(kg/m^2$-sec)
h_a	Heat convection coefficient to ambient, Btu/sec-ft^2-deg R (Cal/m^2-sec-deg K)
h_c	Heat convection coefficient to catalyst particles, Btu/sec-ft^2-deg R (Cal/m^2-sec-deg K)
h_i	Enthalpy, Btu/lb (Cal/kg)
$h_i^{(s)}$	Enthalpy at the Ice/Ice-Liquid interface, Btu/lb (Cal/kg)
$h_i^{(s-\ell)}$	Enthalpy at the Ice-Liquid/Liquid interface, Btu/lb (Cal/kg)
$h_i^{(\ell)}$	Enthalpy at the Liquid/Liquid-Vapor interface, Btu/lb (Cal/kg)
$h_i^{(\ell-v)}$	Enthalpy at the Liquid-Vapor/Vapor interface, Btu/lb (Cal/kg)
h_w	Heat transfer coefficient at reactor wall, Btu/sec-ft^2-deg R (Cal/m^2-sec-deg K)
H'	Heat of reaction, (negative for exothermic reaction), Btu/lb (Cal/kg)
H'_I	Heat of reaction, Btu/lb of species I (Cal/kg of species I)
ΔH^c	Heat of condensation, Btu/lb (Cal/kg)
ΔH^f	Heat of fusion, Btu/lb (Cal/kg)
i	Moles of species I
I	Symbol for general species I
k_c	Mass convection coefficient, ft/sec (m/sec)
k_p	Thermal conductivity of catalyst particle, Btu/ft-sec-deg R (Cal/m-sec-deg K)
K	Thermal conductivity of the interstitial fluid, Btu/ft-sec-deg R (Cal/m-sec-deg K)
L	Length of reactor, ft(m)

m_w	Thermal mass of reactor, lb(kg)
M	Molecular weight, lb/lb mole (kg/kg mole)
$\overline{M}$	Average molecular weight, lb/lb mole (kg/kg mole)
n	Integer values: 1, 2, 3, ... etc.
$\mathbb{N}$	Roots of characteristic equation; see Eq. (I-13)
P	Chamber pressure, psia (N/m^2)
r'	Rate of (Heterogeneous) chemical reaction on the catalyst surfaces, lb/ft^3-sec (kg/m^3-sec)
r_{hom}	Rate of (Homogeneous) chemical reaction in the interstitial phase, lb/ft^3-sec (kg/m^3-sec)
t	Time, sec
T	Temperature within catalyst particle, deg R (deg K)
T*	Equals $T-T_i$, deg R (deg K)
T_a	Temperature of ambient, deg R (deg K)
T_i	Temperature in interstitial phase, deg R (deg K)
T_w	Temperature of reactor wall, deg R (deg K)
$(T_p)_s$	Temperature at surface of catalyst particle, deg R (deg K)
u	Moles of product species U
U	Symbol for product species U
v	Moles of product species V
V	Symbol for product species V
w_i	Weight fraction of reactant in interstitial phase
x	Radial distance from center of spherical catalyst particle, ft (m)
z	Axial distance, ft (m)
α	Catalytic reaction rate constant, or, diffusivity, equals D_I for mass convection or κ for heat convection, ft^2/sec (m^2/sec)
κ	Thermal diffusivity, ft^2/sec (m^2/sec)
δ	Interparticle void fraction
μ	Viscosity of interstitial fluid, lb/ft-sec (kg/m-sec)
ρ_i	Density of interstitial fluid, lb/ft^3 (kg/m^3)
ρ_I	Mass concentration of gas species I within the porous catalyst particle, lb/ft^3 (kg/m^3)
ρ_{I*}	Equals $\rho_I - (\rho_I)_i$, lb/ft^3 (kg/m^3)
ρ_p	Bulk density of catalyst particle, lb/ft^3 (kg/m^3)
$(\rho_I)_i$, $(\rho_J)_i$	Mass concentration of species I, J in interstitial fluid, lb/ft^3 (kg/m^3)
ϕ	Equals $(k_c)_I/D_I$ for mass convection, or, equals h_c/k_p for heat convection, ft^{-1} (m^{-1})

Subscripts

a	Refers to ambient conditions
A	Refers to primary reactant species A
B	Refers to reactant species B

c	Refers to water within the catalyst particle in condensed form
F	Refers to feed
H_2	Refers to hydrogen
H_2O	Refers to water
i	Refers to interstitial gas phase
I	Refers to general species I
J	Refers to general species J
NC	Refers to rate of reaction when no condensed water is formed
o	Refers to source system (x_o, t_o) of the Green's function, or, initial value
O_2	Refers to oxygen
p	Refers to catalyst particle
s	Refers to surface of catalyst particle
T	Refers to temperature
U	Refers to product species U
V	Refers to product species V
w	Refers to reactor wall

Superscripts

(ℓ)	Refers to liquid phase
(s)	Refers to solid phase
(v)	Refers to vapor phase

APPENDIX I

Derivation of Integral Equations Representing Transient Temperature and Concentration Profiles Within a Porous Catalyst Particle Surrounded by a Gas Film

In this section a mathematical model of the simultaneous processes of diffusion, heat transfer, and chemical reaction occurring within individual catalyst particles under transient conditions is described. The system considered in this model is a porous catalyst particle which is represented as an "equivalent" sphere with a diameter taken as a function of the particle size and shape. The catalyst particle is assumed to be surrounded by a stagnant film of gas through which reactant molecules must diffuse before diffusing into the interstices of the porous particle and reacting on the catalytic surfaces.

In developing this analysis, a single reaction involving multiple chemical species is considered where

$$aA + bB + \cdots \longrightarrow uU + vV + \cdots \qquad \text{(I-1)}$$

A, B, --- and U, V, --- represent the reactant and product species respectively and a, b, --- u, v, --- represent the moles of reactants and products for stoichiometric balance. It is apparent that the rate of chemical reaction can be expressed in terms of any of the reactants or products. However, the rate may be a function of the concentrations of any or all of the species and temperature, such that

$$r_I' = F(\rho_A, \rho_B, \cdots, \rho_I, \cdots \rho_U, \rho_V, \cdots T) \qquad \text{(I-2)}$$

In describing the diffusion of mass within the porous particle, it is assumed that Fick's law can be applied by using effective diffusion coefficients to represent the "average" diffusion of the chemical species and that spatial variations in the mass density of the gas are negligible compared to spatial variations in the mass concentrations. Assuming the effective diffusion coefficients to be spatially uniform, the equations describing transient mass transfer of reactant and product gases within the porous catalyst particle may be written as

$$\frac{D_A}{x^2}\frac{\partial}{\partial x}\left(x^2\frac{\partial \rho_A^*}{\partial x}\right) - \frac{\partial \rho_A^*}{\partial t} = r_A' \qquad \text{(I-3a)}$$

Reactants

$$\frac{D_B}{x^2}\frac{\partial}{\partial x}\left(x^2\frac{\partial \rho_B^*}{\partial x}\right) - \frac{\partial \rho_B}{\partial t} = \frac{bM_B}{aM_A} r_A' \qquad \text{(I-3b)}$$

$$\vdots \qquad \vdots \qquad \vdots$$

$$\frac{D_U}{x^2}\frac{\partial}{\partial x}\left(x^2\frac{\partial \rho_U^*}{\partial x}\right) - \frac{\partial \rho_U^*}{\partial t} = -\frac{uM_U}{aM_A} r_A' \qquad \text{(I-3u)}$$

Products

$$\frac{D_V}{x^2}\frac{\partial}{\partial x}\left(x^2\frac{\partial \rho_V^*}{\partial x}\right)-\frac{\partial \rho_V^*}{\partial t}=-\frac{\nu M_V}{a M_A}r_A' \qquad \text{(I-3v)}$$

⋮ ⋮ ⋮

where

$$\rho_A^*=\rho_A-(\rho_A)_i \qquad \rho_B^*=\rho_B-(\rho_B)_i$$

$$\rho_U^*=\rho_U-(\rho_U)_i \qquad \rho_V^*=\rho_V-(\rho_V)_i$$

In describing the transfer of heat within the catalyst particle, it is assumed that energy transfer by mass diffusion may be neglected, that viscous and pressure work can be ignored, and that the particle structure is the primary heat conduction and heat storage media. By applying Fourier's law and assuming the effective thermal conductivity is spatially uniform, the equation describing transient heat transfer within the porous catalyst particle may be written as

$$\frac{k_p}{x^2}\frac{\partial}{\partial x}\left(x^2\frac{\partial T^*}{\partial x}\right)-\rho_p C_p\frac{\partial T^*}{\partial t}=H_A' r_A' \qquad \text{(I-4)}$$

where $T^*=T-T_i$

The boundary conditions which consider diffusion of heat and mass through a gas film surrounding the catalyst particle are

$$\frac{\partial \rho_A^*}{\partial x}(a,t)=-\phi_A \rho_A^*(a,t) \qquad \text{(I-5a)}$$

Reactants

$$\frac{\partial \rho_B^*}{\partial x}(a,t)=-\phi_B \rho_B^*(a,t) \qquad \text{(I-5b)}$$

⋮ ⋮ ⋮

$$\frac{\partial \rho_U^*}{\partial x}(a,t)=-\phi_U \rho_U^*(a,t) \qquad \text{(I-5u)}$$

Products

$$\frac{\partial \rho_V^*}{\partial x}(a,t) = -\phi_V \rho_V^*(a,t) \qquad \text{(I-5v)}$$

$$\frac{\partial T^*}{\partial x}(a,t) = -\phi_T T^*(a,t) \qquad \text{(I-6)}$$

where $\phi_I = \dfrac{(k_c)_I}{D_I}$ for mass convection with $I = A, B, \cdots, U, V \cdots \quad I \neq T$

and $\phi_T = \dfrac{h_c}{K_p}$ for heat convection.

The initial conditions are taken as general functions of position with

$$\rho_A^*(x,0) = \rho_A^*(x)_0 \qquad \text{(I-7a)}$$

Reactants

$$\rho_B^*(x,0) = \rho_B^*(x)_0 \qquad \text{(I-7b)}$$

$$\rho_U^*(x,0) = \rho_U^*(x)_0 \qquad \text{(I-7u)}$$

Products

$$\rho_V^*(x,0) = \rho_V^*(x)_0 \qquad \text{(I-7v)}$$

and

$$T^*(x,0) = T^*(x)_0 \qquad \text{(I-8)}$$

With a knowledge of the reaction kinetics the system is completely defined. Equations (I-3) through (I-8) can be solved, together with an expression for the rate of chemical reaction, r'_A, to determine concentration and temperature distributions within the catalyst particle as a function of position and time. The

simultaneous solution to these equations can be accomplished by converting Eqs. (I-3) and (I-4) together with the boundary and initial conditions given by Eqs. (I-5) through (I-8) into a set of implicit integral equations.

It may be noted that Eqs. (I-3) and (I-4) are a set of simultaneous, non-homogeneous partial differential equations, each describing a different scalar diffusion function. Using Green's function techniques (Ref. 10) the non-homogeneous diffusion equation can be converted to an implicit integral equation. Similar techniques have been employed to solve a non-homogeneous steady-state diffusion equation in Ref 11 and a set of simultaneous non-homogeneous transient diffusion equations in Ref. 12. Integral equations representing the primary reactant concentration, the other reactant concentrations, the product concentrations, and temperature within a spherical catalyst particle can be obtained using the methods developed in Ref. 12 as

$$\rho_A^*(x,t) = -\frac{1}{4\pi D_A}\int_0^{t^+} dt_o \int_0^a dx_o \; x_o^2 \; r_A'(x_o,t_o)\, G_A(x,t/x_o,t_o) + \frac{1}{4\pi D_A}\int_0^a dx_o \; x_o^2 \left[\rho_A^* G_A\right]_{t_o=0} \tag{I-9}$$

where t^+ is chosen infinitesimally greater than t (cf Ref. 12).

$$\rho_B^*(x,t) = -\frac{1}{4\pi D_B}\frac{bM_B}{aM_A}\int_0^{t+} dt_o \int_0^a dx_o\, x_o^2\, r_A'(x_o,t_o)\, G_B(x,t/x_o,t_o) + \frac{1}{4\pi D_B}\int_0^a dx_o\, x_o^2 \left[\rho_B^* G_B\right]_{t_o=0} \tag{I-10}$$

$$\rho_U^*(x,t) = \frac{1}{4\pi D_U}\frac{uM_U}{aM_A}\int_0^{t^+} dt_o \int_0^a dx_o\, x_o^2\, r_A'(x_o,t_o)\, G_U(x,t/x_o,t_o) + \frac{1}{4\pi D_U}\int_0^a dx_o\, x_o^2 \left[\rho_U^* G_U\right]_{t_o=0} \tag{I-11}$$

$$T^*(x,t) = -\frac{1}{4\pi}\frac{H_A'}{kp}\int_0^{t^+} dt_o \int_0^a dx_o\, x_o^2\, r_A'(x_o,t_o)\, G_T(x,t/x_o,t_o) + \frac{1}{4\pi\kappa}\int_0^a dx_o\, x_o^2 \left[T^* G_T\right]_{t_o=0} \tag{I-12}$$

Using Laplace transform methods the Green's functions are found to be

$$G_I(x,t/x_o,t_o) = \frac{8\pi a_I}{a}\left(\frac{x_o}{x}\right)\sum_{n=1}^{\infty}\frac{N_n^2+(\phi_I a-1)^2}{N_n^2+\phi_I a(\phi_I a-1)} \qquad \text{(I-13)}$$

$$\cdot \sin\left(N_n\frac{x}{a}\right)\quad \sin\left(N_n\frac{x_o}{a}\right) e^{-\left(\frac{N_n}{a}\right)^2 a_I (t-t_o)}$$

where I = A, B, ---, T, U, V, ---, and the N_n are the positive roots of the characteristic equation

$$N_n \cot N_n + (\phi_I a-1) = 0$$

a_I and ϕ_I are the appropriate diffusion constants expressed as follows:

For mass transfer $\quad a_I = D_I \quad$ and $\quad \phi_I = \frac{(k_c)_I}{D_I}$

For heat transfer $\quad a_I = \kappa \quad$ and $\quad \phi_I = \frac{h_c}{K_p}$

Numerical methods must be employed to solve Eqs. (I-9) through (I-12) simultaneously for the chemical species concentrations and temperature as functions of time and position within the catalyst particle. By applying the mean value theorem to the time integrals which involve the rate of reaction, Eqs. (I-9) through (I-12) can be rewritten as

$$\rho_A^*(x,t) = -\frac{1}{4\pi D_A}\int_0^a x_o^2\, r_A'(x_o,\xi)\int_0^{t^+} G_A(x,t/x_o,t_o)\,dt_o\,dx_o \qquad \text{(I-14)}$$

$$+\frac{1}{4\pi D_A}\int_0^a x_o^2 \rho_A^*(x_o,0)\, G_A(x,t/x_o,0)\,dx_o$$

$$\rho_B^*(x,t) = -\frac{1}{4\pi D_B}\,\frac{bM_b}{aM_a}\int_0^a x_o^2\, r_A'(x_o,\xi)\int_0^{t^+} G_B(x,t/x_o,t_o)\,dt_o\,dx_o \qquad \text{(I-15)}$$

$$+\frac{1}{4\pi D_B}\int_0^a x_o^2 \rho_B^*(x_o,0)\, G_B(x,t/x_o,0)\,dx_o$$

$$\rho_U^*(x,t) = \frac{1}{4\pi D_U}\frac{uM_U}{aM_A}\int_0^a x_0^2\, r_A'(x_0,\xi)\int_0^{t^+} G_U(x,t/x_0,t_0)\,dt_0\,dx_0 + \frac{1}{4\pi D_U}\int_0^a \rho_U^*(x_0,0)\,G_U(x,t/x_0,0)\,dx_0 \qquad \text{(I-16)}$$

$$T^*(x,t) = -\frac{1}{4\pi}\frac{H_A'}{k_p}\int_0^a x_0^2\, r_A'(x_0\xi)\int_0^{t^+} G_T(x,t/x_0;t_0)\,dt_0 dx_0 + \frac{1}{4\pi\kappa}\int_0^a T^*(x_0,0)\,G_T(x,t/x_0,0)\,dx_0 \qquad \text{(I-17)}$$

The mean rate of reaction with respect to time, $r'_A(X_0, \xi)$, is obtained from the mean value theorem as

$$r_A'(x_0,\xi) = \frac{\int_0^{t^+} r_A'(x_0,t_0)\,G_I(x,t/x_0,t_0)\,dt_0}{\int_0^{t^+} G_I(x,t/x_0,t_0)\,dt_0} \qquad \text{where} \qquad 0 \le \xi \le t^+ \qquad \text{(I-18)}$$

To facilitate the numerical procedure it is convenient to integrate over time intervals which are sufficiently short so that the rate of reaction, $r'_A(X_0, t_0)$, can be assumed to vary linearly with time. In the source coordinate system, the rate of reaction over a short time interval 0 to t^+ can be written as

$$r_A'(x_0,t_0) = \left[r_A'(x_0,t^+) - r_A'(x_0,0)\right]\frac{t_0}{t^+} + r_A'(x_0,0) \qquad \text{(I-19)}$$

By combining Eqs. (I-18) and (I-19) the mean time, ξ, can be obtained as

$$\xi = \frac{\int_0^{t^+} t_0 G_I(x,t/x_0,t_0)\,dt_0}{\int_0^{t^+} G_I(x,t/x_0,t_0)\,dt_0} \qquad \text{(I-20)}$$

Then by substituting Eqs. (I-19) and (I-20) into Eqs. (I-14) through (I-17), the chemical species concentration and temperature profiles at the end of a time interval, t, are obtained as

$$\rho_A^*(x,t) = -\frac{1}{4\pi D_A}\int_0^a x_0^2 \left\{\left[\frac{r_A'(x_0,t) - r_A'(x_0,0)}{t}\right]\int_0^t t_0 G_A(x,t/x_0,t_0)\,dt_0 + r_A'(x_0,0)\int_0^t G_A(x,t/x_0,t_0)\,dt_0 - \rho_A^*(x_0,0)\,G_A(x,t/x_0,0)\right\} dx_0 \qquad \text{(I-21)}$$

$$\rho_B^*(x,t) = -\frac{1}{4\pi D_B}\int_0^a x_0^2 \left\{ \frac{bM_B}{aM_A}\left[\frac{r_A'(x_0,t)-r_A'(x_0,0)}{t}\right]\int_0^t t_0 G_B(x,t/x_0,t_0)\,dt_0 + \frac{bM_B}{aM_A} r_A'(x_0,0)\int_0^t G_B(x,t/x_0,t_0)\,dt_0 - \rho_B^*(x_0,0)\,G_B(x,t/x_0,0)\right\} dx_0 \quad \text{(I-22)}$$

$$\rho_U^*(x,t) = \frac{1}{4\pi D_U}\int_0^a x_0^2 \left\{ \frac{uM_U}{aM_A}\left[\frac{r_A'(x_0,t)-r_A'(x_0,0)}{t}\right]\int_0^t t_0 G_U(x,t/x_0,t_0)\,dt_0 + \frac{uM_U}{aM_A} r_A'(x_0,0)\int_0^t G_U(x,t/x_0,t_0)\,dt_0 + \rho_U^*(x_0,0)\;G_U(x,t/x_0,0)\right\} dx_0 \quad \text{(I-23)}$$

$$T^*(x,t) = -\frac{1}{4\pi\kappa}\int_0^a x_0^2 \left\{ \frac{H_A'\kappa}{k_p}\left[\frac{r_A'(x_0,t)-r_A'(x_0,0)}{t}\right]\int_0^t t_0 G_T(x,t/x_0,t_0)\,dt_0 + \frac{H_A'\kappa}{k_p} r_A'(x_0,0)\int_0^t G_T(x,t/x_0,t_0)\,dt_0 - T^*(x_0,0)\,G_T(x,t/x_0,0)\right\} dx_0 \quad \text{(I-24)}$$

It should be noted that Eqs. (I-21) through (I-24) for the concentrations and temperature profiles at time, t, involve only spatial integrals since the time integrals can be evaluated in closed form.

The above equations can be used to solve numerically for the concentration and temperature profiles within a catalyst particle as functions of time by representing the transient as a series of successive short time intervals. The time intervals are taken sufficiently short such that the rate of reaction is essentially linear during each time interval. Concentrations and temperatures computed at each value of time become the initial conditions for the computations pertinent to the subsequent time.

APPENDIX II

DISTRIBUTION LIST FOR FINAL REPORT
(Contract NAS 3-13317)

Addressee	Copies of Final Report	Copies of Computer Manual
National Aeronautics & Space Administration Lewis Research Center 21000 Brookpark Road Cleveland, Ohio 44135		
Attn: Contracting Officer, MS 500-313	1	1
Attn: E. A. Bourke, MS 500-203	5	1
Attn: Technical Report Control Office MS 5-5	1	1
Attn: Technology Utilization Office MS 3-16	1	1
Attn: AFSC Liaison Office, 501-3	2	1
Attn: Library	2	1
Attn: Office of Reliability & Quality Assurance MS 500-111	1	
Attn: D. L. Nored, Chief, LRTB MS 500-209	1	
Attn: P. N. Herr, Project Manager MS 500-209	6	1
Attn: E. W. Conrad, MS 500-204	1	
Attn: R. H. Kemp, MS 49-1	1	
Attn: R. H. Knoll, MS 501-2	1	
Attn: J. W. Gregory, MS 500-209	1	

DISTRIBUTION LIST FOR FINAL REPORT
(Contract NAS 3-13317)

Addressee	Copies of Final Report	Copies of Computer Manual
Chief, Liquid Experimental Engineering, RPX Office of Advanced Research & Technology NASA Headquarters Washington, D.C. 20546	2	1
Chief, Liquid Propulsion Technology, RPL Office of Advanced Research & Technology NASA Headquarters Washington, D.C. 20546	2	
Director, Launch Vehicles & Propulsion, SV Office of Space Science & Applications NASA Headquarters Washington, D.C. 20546	1	1
Chief, Environmental Factors & Aerodynamics Code RV-1 Office of Advanced Research & Technology NASA Headquarters Washington, D.C. 20546	1	
Director, Advanced Manned Missions, MT Office of Manned Space Flight NASA Headquarters Washington, D.C. 20546	1	1
NASA Scientific & Technical Information Facility P. O. Box 33 College Park, Maryland 20740	6	1
Director, Technology Utilization Division Office of Technology Utilization NASA Headquarters Washington, D.C. 20546	1	

DISTRIBUTION LIST FOR FINAL REPORT
(Contract NAS 3-13317)

	Copies of Final Report	Copies of Computer Manual
National Aeronautics & Space Administration Ames Research Center Moffett Field, California 94035		
Attn: Library	1	1
Attn: Hans M. Mark Mission Analysis Division	*	
National Aeronautics & Space Administration Flight Research Center P. O. Box 273 Edwards, California 93523		
Attn: Library	1	
National Aeronautics & Space Administration Goddard Space Flight Center Greenbelt, Maryland 20771		
Attn: Library	1	
Attn: Merland L. Moseson Code 620	*	
National Aeronautics & Space Administration John F. Kennedy Space Center Cocoa Beach, Florida 32931		
Attn: Library	1	
Attn: Dr. Kurt H. Debus	*	
National Aeronautics & Space Administration Langley Research Center Langley Station Hampton, Virginia 23365		
Attn: Library	1	1
Attn: E. Cortwright, Director	*	

*Letter of transmittal only

DISTRIBUTION LIST FOR FINAL REPORT
(Contract NAS 3-13317)

Addressee	Copies of Final Report	Copies of Computer Manual
National Aeronautics & Space Administration Manned Spacecraft Center Houston, Texas 77001		
Attn: Library	1	1
Attn: J. G. Thiobodaux, Jr. Chief, Propulsion & Power Division	1	1
National Aeronautics & Space Administration George C. Marshall Space Flight Center Huntsville, Alabama 35812		
Attn: Library	1	1
Attn: Hans G. Paul	1	1
Jet Propulsion Laboratory 4800 Oak Grove Drive Pasadena, California 91103		
Attn: Library	1	1
Attn: Duane Dipprey	1	1
Defense Documentation Center Cameron Station Building 5 5010 Duke Street Alexandria, Virginia 22314		
Attn: TISIA	1	
Office of the Director of Defense Research & Engineering Washington, D.C. 20301		
Attn: Office of Asst. Dir. (Chem. Technology)	1	

DISTRIBUTION LIST FOR FINAL REPORT
(Contract NAS 3-13317)

Addressee	Copies of Final Report	Copies of Computer Manual
RTD (RTNP) Bolling Air Force Base Washington, D.C. 20332	1	
Arnold Engineering Development Center Air Force Systems Command Tullahoma, Tennessee 37389		
Attn: Library	1	
Attn: Dr. H. K. Doetsch	*	
Advanced Research Projects Agency Washington, D.C. 20525		
Attn: Library	1	
Aeronautical Systems Division Air Force Systems Command Wright-Patterson Air Force Base Dayton, Ohio		
Attn: Library	1	1
Attn: D. L. Schmidt Code ARSCNC-2	*	
Air Force Rocket Propulsion Laboratory (RPR) Edwards, California 93523		
Attn: Library	1	1
Air Force Office of Scientific Research Washington, D.C. 20333		
Attn: Library	1	1
Attn: SREP, Dr. J. F. Masi	*	

*Letter of transmittal only

DISTRIBUTION LIST FOR FINAL REPORT
(Contract NAS 3-13317)

Addressee	Copies of Final Report	Copies of Computer Manual
Space & Missile Systems Organization Air Force Unit Post Office Los Angeles, California 90045		
Attn: Technical Data Center	1	1
U. S. Army Missile Command Redstone Scientific Information Center Redstone Arsenal, Alabama 35808		
Attn: Document Section	1	1
Attn: Dr. W. Wharton	*	
Bureau of Naval Weapons Department of the Navy Washington, D.C.		
Attn: Library	1	1
Attn: J. Kay Code RTMS-41	*	
Director (Code 6180) U. S. Naval Research Laboratory Washington, D.C. 20390		
Attn: Library	1	
Attn: H. W. Carhart	*	
Attn: J. H. Krafft	*	
Picatinny Arsenal Dover, New Jersey 07801		
Attn: Library	1	
Attn: I. Forsten	*	

*Letter of transmittal only

DISTRIBUTION LIST FOR FINAL REPORT
(Contract NAS 3-13317)

Addressee	Copies of Final Report	Copies of Computer Manual
Air Force Aero Propulsion Laboratory Research & Technology Division Air Force Systems Command United States Air Force Wright-Patterson AFB, Ohio 45433		
Attn: APRP (Library)	1	
Attn: R. Quigley	*	
Attn: C. M. Donaldson	*	
Aerojet Liquid Rocket Company P. O. Box 15847 Sacramento, California 95813		
Attn: Technical Library 2484-2015A	1	1
Attn: R. Stiff	*	
Attn: S. Rosenburg	1	1
Aeroneutronic Division of Philco Ford Corp. Ford Road Newport Beach, California 92663		
Attn: Technical Information Department	1	
Attn: Dr. L. H. Linder	*	
Aerospace Corporation 2400 E. El Segundo Boulevard Los Angeles, California 90045		
Attn: Library-Documents	1	1

*Letter of transmittal only

DISTRIBUTION LIST FOR FINAL REPORT
(Contract NAS 3-13317)

Addressee	Copies of Final Report	Copies of Computer Manual
ARO, Incorporated Arnold Engineering Development Center Arnold AF Station, Tennessee 37389		
Attn: Library	1	
Susquehanna Corporation Atlantic Research Division Shirley Highway & Edsall Road Alexandria, Virginia 22314		
Attn: Library	1	1
Boeing Company Space Division P. O. Box 868 Seattle, Washington 98124		
Attn: Library	1	1
Attn: J. D. Alexander	*	
Attn: C. F. Tiffany	*	
Boeing Company 1625 K Street, N.W. Washington, D. C. 20006	1	
Chemical Propulsion Information Agency Applied Physics Laboratory 8621 Georgia Avenue Silver Spring, Maryland 20910	1	1
Attn: Tom Reedy	*	

*Letter of transmittal only

DISTRIBUTION LIST FOR FINAL REPORT
(Contract NAS 3-13317)

Addressee	Copies of Final Report	Copies of Computer Manual
Chrysler Corporation Space Division P. O. Box 29200 New Orleans, Louisiana 70129		
Attn: Librarian	1	
Research Center Fairchild Hiller Corporation Germantown, Maryland		
Attn: Library	1	1
Attn: Ralph Hall	*	
Republic Aviation Fairchild Hiller Corporation Farmington, Long Island New York	1	1
General Dynamics/Convair P. O. Box 1128 San Diego, California 92112		
Attn: Library	1	1
Attn: Frank Dore	*	
Missiles and Space Systems Center General Electric Company Valley Forge Space Technology Center P. O. Box 8555 Philadelphia, Pennsylvania 19101		
Attn: Library	1	1
Attn: A. Cohen	*	
Attn: F. Schultz	*	

*Letter of transmittal only

DISTRIBUTION LIST FOR FINAL REPORT
(Contract NAS 3-13317)

Addressee	Copies of Final Report	Copies of Computer Manual
General Electric Company Flight Propulsion Lab. Department Cincinnati, Ohio		
Attn: Library	1	
Attn: D. Suichu	*	
Attn: Leroy Smith	*	
Grumman Aircraft Engineering Corporation Bethpage, Long Island, New York		
Attn: Library	1	
Attn: Joseph Gavin	1	1
Honeywell Inc. Aerospace Division 2600 Ridgeway Road Minneapolis, Minnesota		
Attn: Library	1	1
Attn: C. K. Hersh	*	
Kidde Aerospace Division Walter Kidde & Company, Inc. 567 Main Street Belleville, New Jersey 07107	1	1
Attn: R. J. Hanville	*	
Ling-Temco-Vought Corporation P. O. Box 5907 Dallas, Texas 75222		
Attn: Library	1	

*Letter of transmittal only

DISTRIBUTION LIST FOR FINAL REPORT
(Contract NAS 3-13317)

Addressee	Copies of Final Report	Copies of Computer Manual
Lockheed Missiles and Space Company P. O. Box 504 Sunnyvale, California 94087		
Attn: Library	1	1
Marquardt Corporation 16555 Saticoy Street Box 2013 - South Annex Van Nuys, California 91409	1	1
Attn: T. Hudson	*	
Rocket Research Corporation Willow Road at 116th Street Redmond, Washington 98052		
Attn: Library	1	
Attn: F. McCullough, Jr.	1	1
Attn: D. Emmonds	1	1
TRW Systems Inc. 1 Space Park Redondo Beach, California 90278		
Attn: Tech. Lib. Doc. Acquisitions	1	1
Attn: D. H. Lee	*	
Attn: R. J. Johnson	1	1

*Letter of transmittal only

DISTRIBUTION LIST FOR FINAL REPORT
(Contract NAS 3-13317)

Addressee	Copies of Final Report	Copies of Computer Manual
United Aircraft Corporation Pratt & Whitney Division Florida Research & Development Center P. O. Box 2691 West Palm Beach, Florida 33402		
Attn: Library	1	1
Attn: R. J. Coar	*	
Attn: Dr. Schmitke	*	
Denver Division Martin-Marietta Corporation P. O. Box 179 Denver, Colorado 80201		
Attn: Library	1	1
Attn: Dr. Morganthaler	*	
Attn: F. R. Schwartzberg	*	
Western Division McDonnell Douglas Astronautics 5301 Bolsa Avenue Huntington Beach, California 92647		
Attn: Library	1	1
Attn: R. W. Hallet	*	
Attn: G. W. Burge	*	
Attn: P. Klevatt	*	

*Letter of transmittal only

DISTRIBUTION LIST FOR FINAL REPORT
(Contract NAS 3-13317)

Addressee	Copies of Final Report	Copies of Computer Manual
McDonnell Douglas Aircraft Corporation P. O. Box 516 Lambert Field, Missouri 63166		
Attn: Library	1	1
Attn: R. A. Herzmark	*	
Rocketdyne Division North American Rockwell Inc. 6633 Canoga Avenue Canoga Park, California 91304		
Attn: Library, Department 596-306	1	1
Attn: Dr. R. J. Thompson	*	
Attn: S. F. Iacobellis	*	
Space & Information Systems Division North American Rockwell 12214 Lakewood Boulevard Downey, California		
Attn: Library	1	1
United Aircraft Corporation United Technology Center P. O. Box 358 Sunnyvale, California 94038		
Attn: Library	1	
Attn: Dr. David Altman	*	

*Letter of transmittal only

DISTRIBUTION LIST FOR FINAL REPORT
(Contract NAS 3-13317)

Addressee	Copies of Final Report	Copies of Computer Manual
Chemical Propulsion Information Agency Applied Physics Laboratory 8621 Georgia Avenue Silver Spring, Maryland 20910	1	
General Dynamics/Convair P. O. Box 1128 San Diego, California 92112		
Attn: Library and Information Services (128-00)	1	
Hamilton Standard Corporation Windsor Locks, Connecticut 06096		
Attn: Library	1	1

FIG. 1

TRANSIENT AXIAL GAS TEMPERATURE PROFILES

NOMINAL CHAMBER PRESSURE = 300 PSIA (2.07×10^6 N/M^2)

FEED TEMPERATURE = 360 DEG R (200 DEG K)

INITIAL BED TEMPERATURE = 360 DEG R (200 DEG K)

FEED MIXTURE RATIO = 1.0 LB O_2/LB H_2 (1.0 KG O_2/KG H_2)

MASS FLOW RATE = 1.05 LB/FT^2-SEC (5.13 KG/M^2 - SEC)

CATALYST PARTICLE SIZE = 14-18 MESH

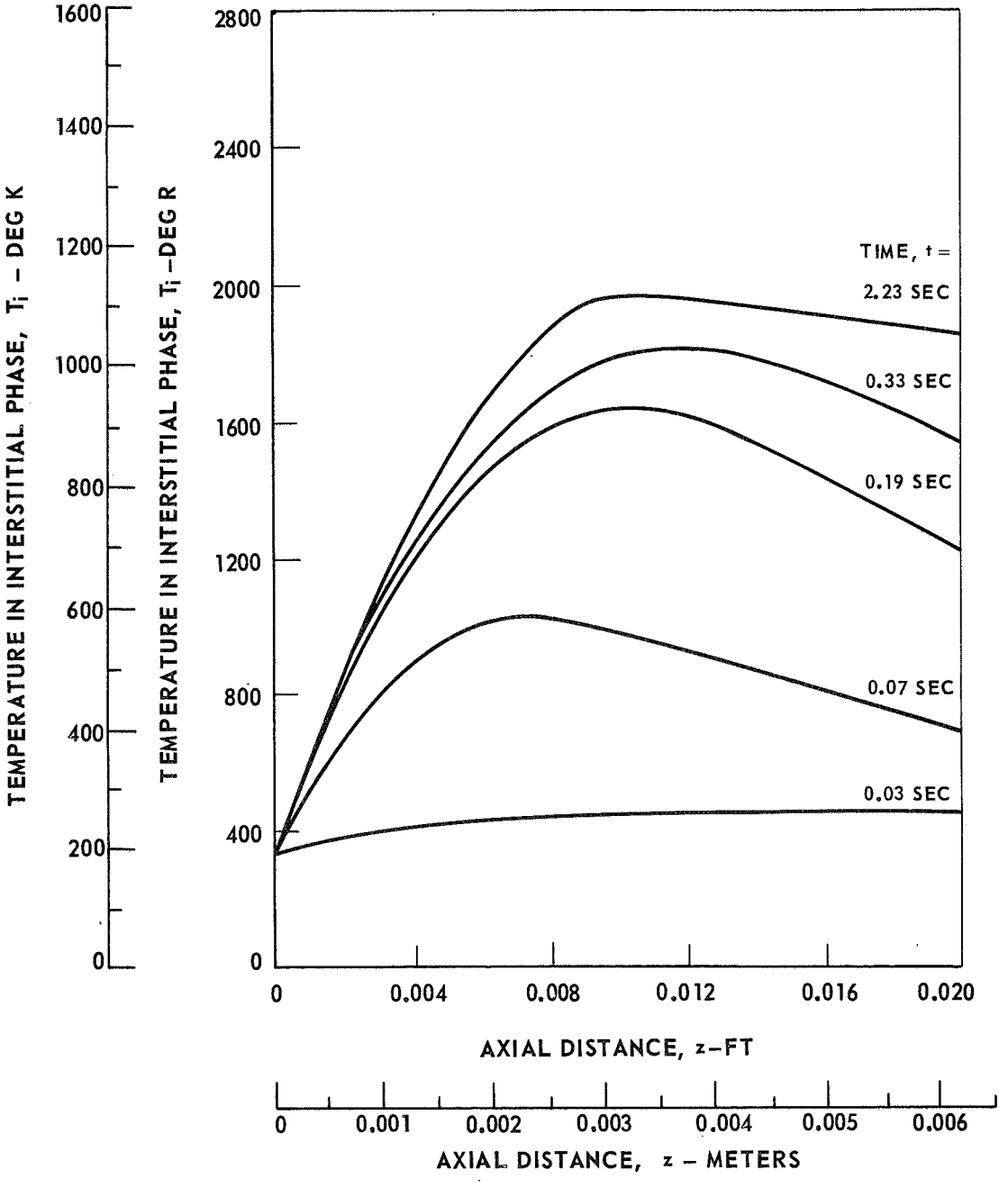

TRANSIENT AXIAL PROFILES OF PARTICLE SURFACE TEMPERATURES

NOMINAL CHAMBER PRESSURE = 300 PSIA (2.07×10^5 N/M^2)
FEED TEMPERATURE = 360 DEG R (200 DEG K)
INITIAL BED TEMPERATURE = 360 DEG R (200 DEG K)
FEED MIXTURE RATIO = 1.0 LB O_2/LB H_2 (1.0 KG O_2/KG H_2)
MASS FLOW RATE = 1.05 LB/FT^2-SEC (5.13 KG/M^2 - SEC)
CATALYST PARTICLE SIZE = 14-18 MESH

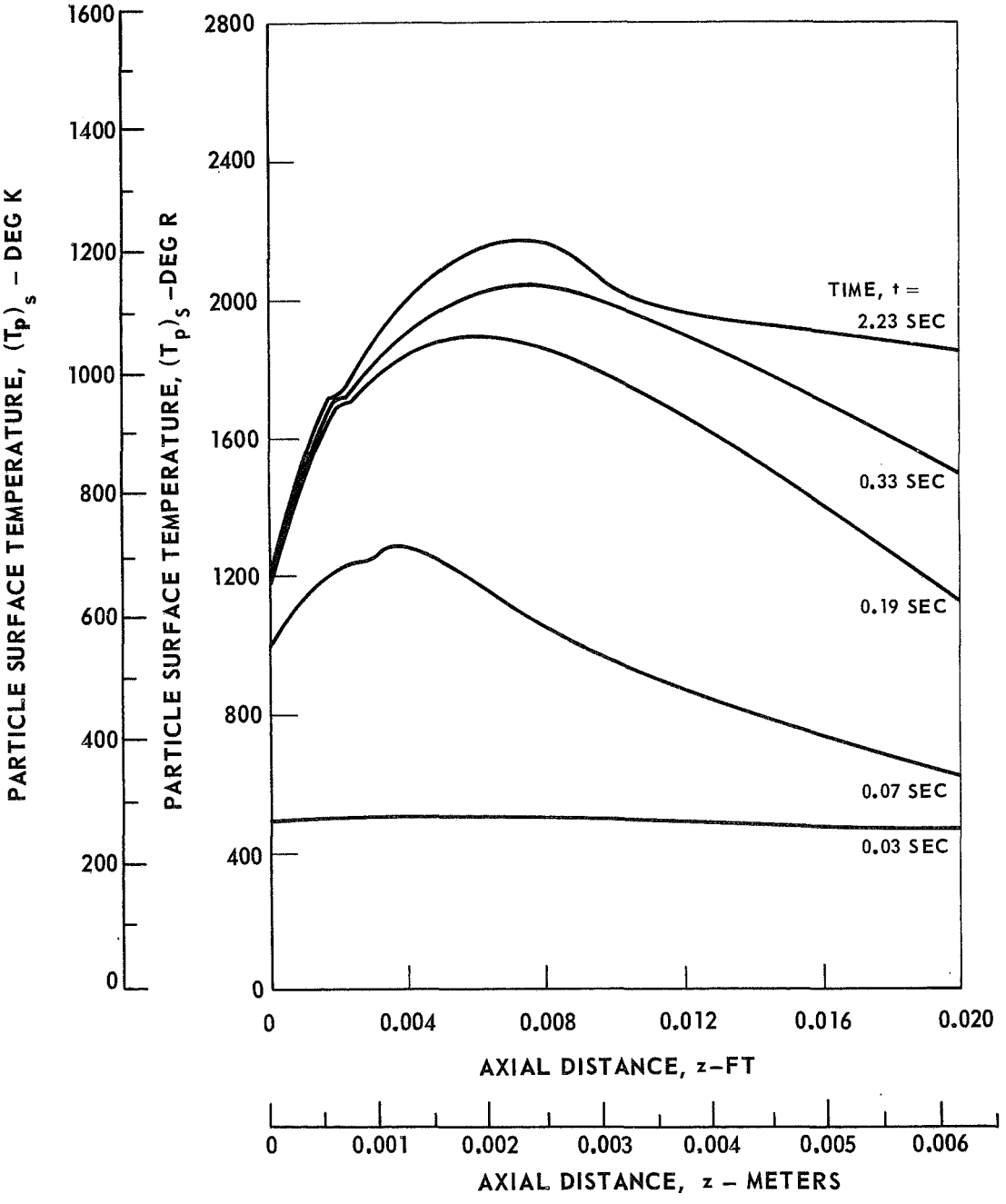

VARIATIONS OF GAS, PARTICLE SURFACE AND WALL TEMPERATURES WITH TIME AT TWO AXIAL POSITIONS

NOMINAL CHAMBER PRESSURE = 300 PSIA (2.07×10^6 N/M 2)
FEED TEMPERATURE = 360 DEG R (200 DEG K)
INITIAL BED TEMPERATURE = 360 DEG R (200 DEG K)
FEED MIXTURE RATIO = 1.0 LB O_2/LB H_2 (1.0 KG O_2/KG H_2)
MASS FLOW RATE = 1.05 LB/FT^2-SEC (5.13 KG/M^2-SEC)
CATALYST PARTICLE SIZE = 14-18 MESH

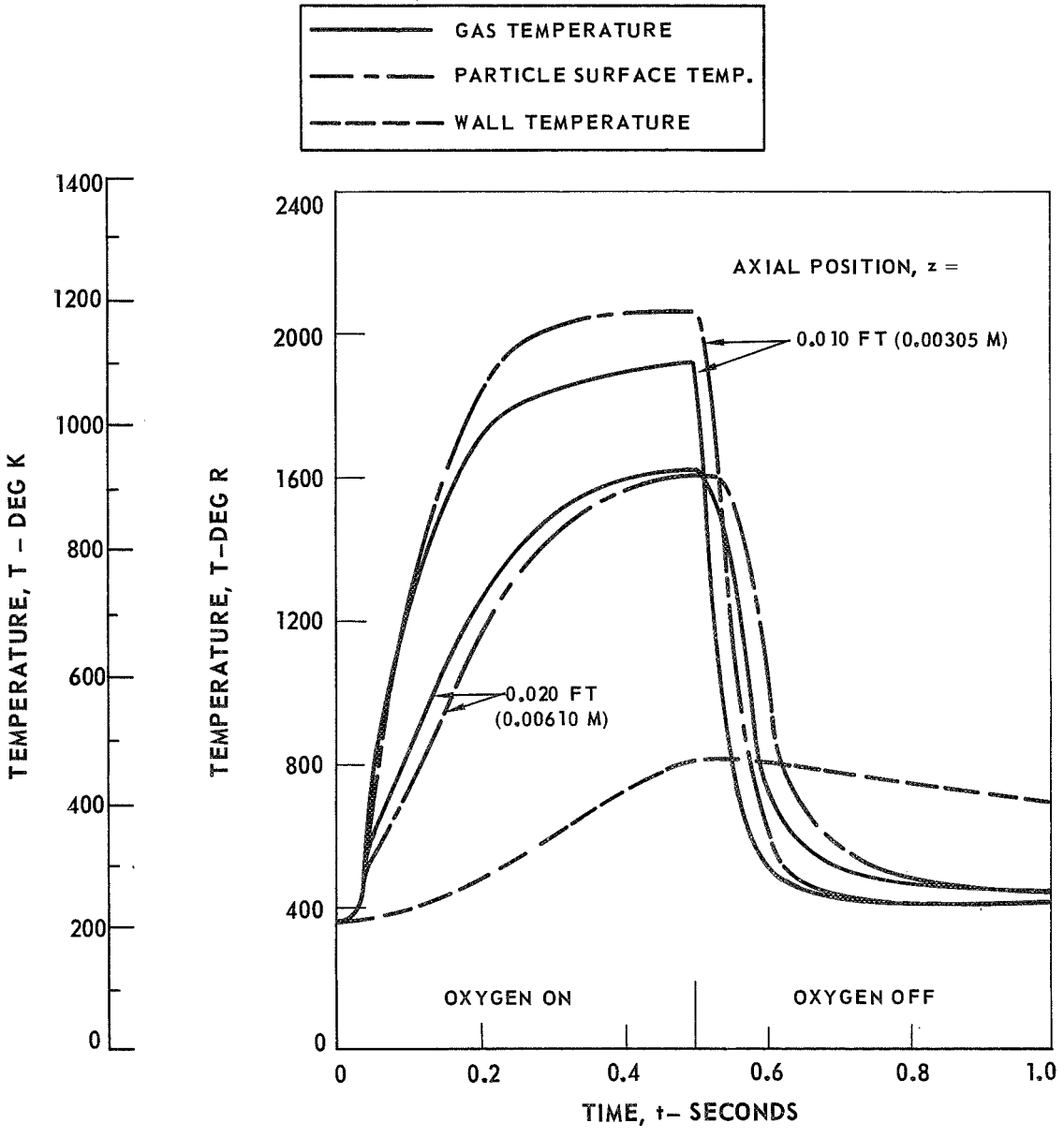

FIG. 4

TRANSIENT AXIAL PROFILES OF MOLE-FRACTION OF OXYGEN IN GAS PHASE

NOMINAL CHAMBER PRESSURE = 300 PSIA (2.07×10^6 N/M^2)

FEED TEMPERATURE = 360 DEG R (200 DEG K)

INITIAL BED TEMPERATURE = 360 DEG R (200 DEG K)

FEED MIXTURE RATIO = 1.0 LB O_2/LB H_2 (1.0 KG O_2 /KG H_2)

MASS FLOW RATE = 1.05 LB/FT^2-SEC (5.13 LB/FT^2 - SEC)

CATALYST PARTICLE SIZE = 14-18 MESH

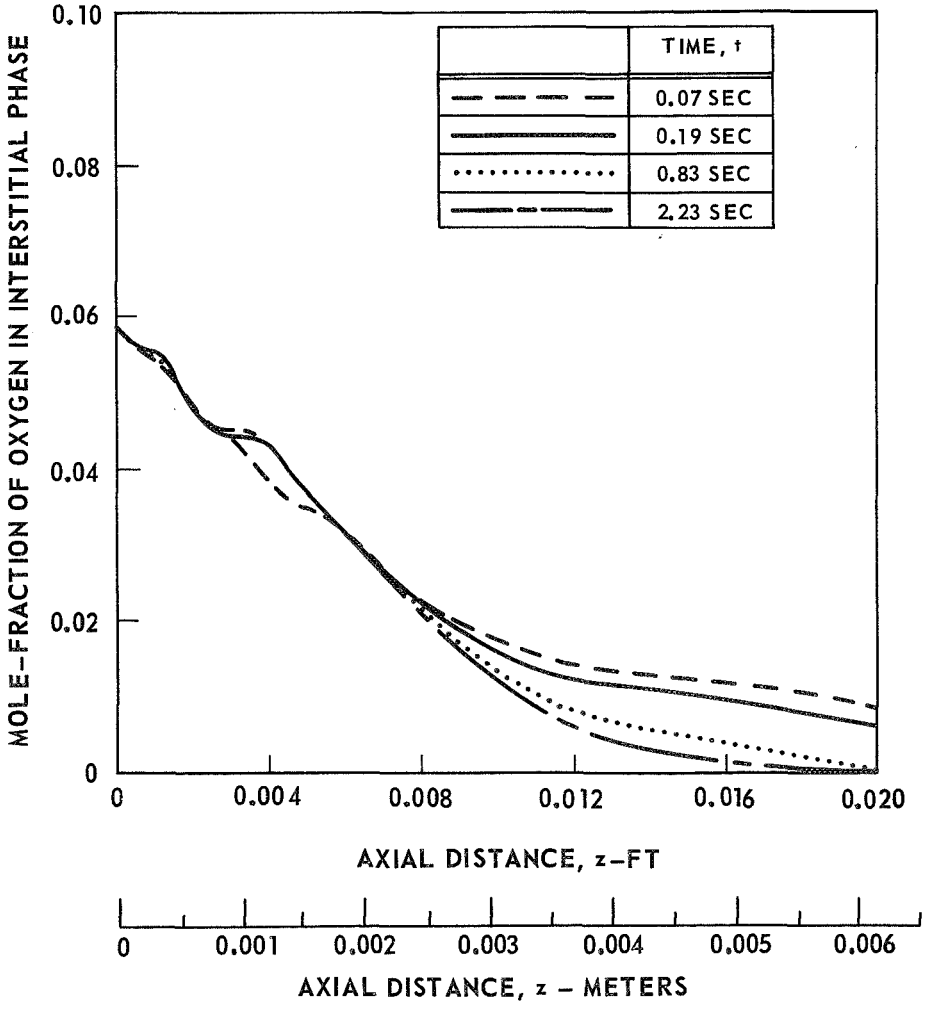

FIG. 5

TRANSIENT AXIAL GAS TEMPERATURE PROFILES

FEED MIXTURE RATIO = 2.0 LB O_2/LB H_2 (2.0 KG O_2/KG H_2)

NOMINAL CHAMBER PRESSURE = 300 PSIA (2.07×10^6 N/M^2)

FEED TEMPERATURE = 360 DEG R (200 DEG K)

INITIAL BED TEMPERATURE = 360 DEG R (200 DEG K)

MASS FLOW RATE = 1.05 LB/FT^2-SEC (5.13 KG/M^2 - SEC)

CATALYST PARTICLE SIZE = 14-18 MESH

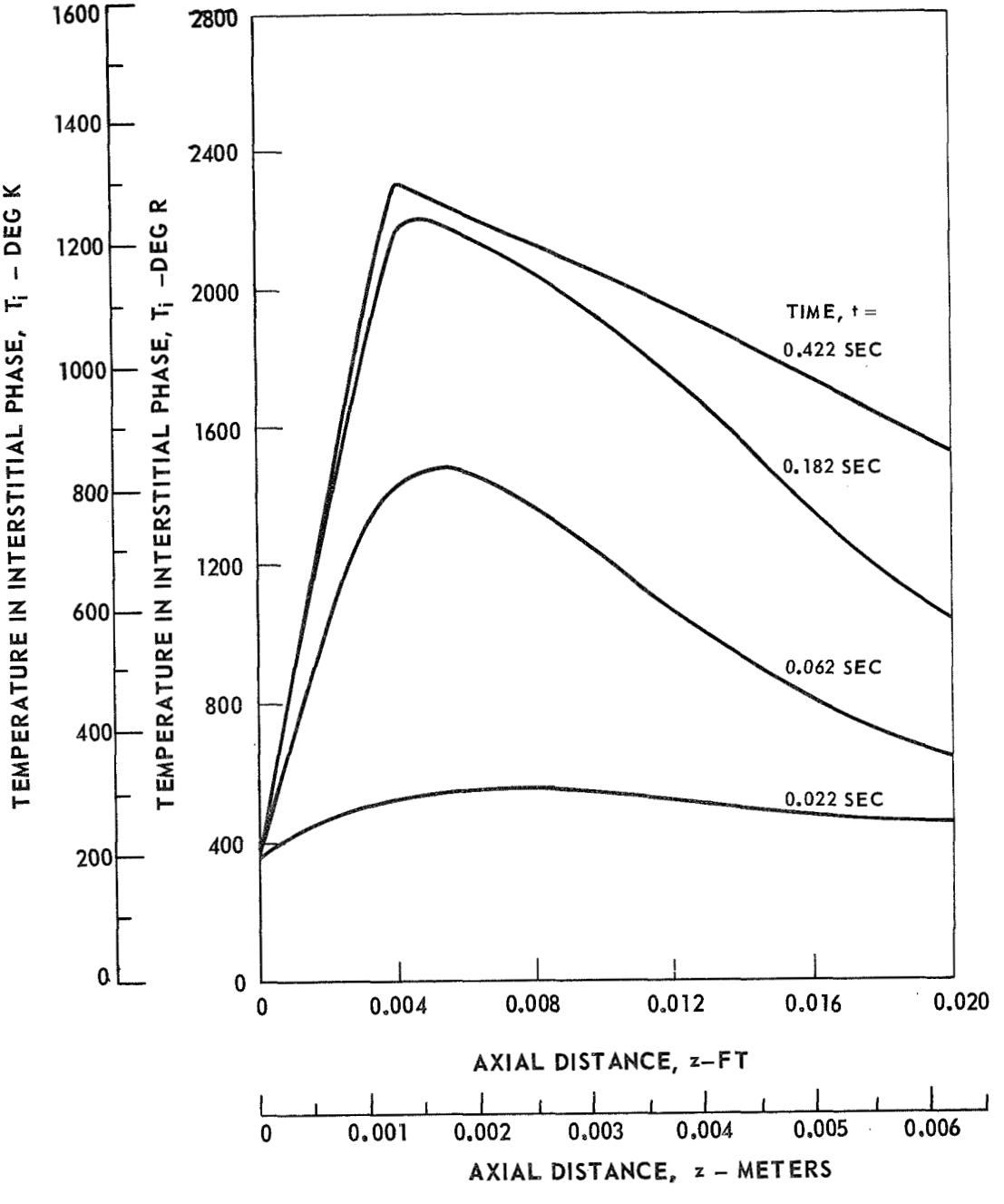

TRANSIENT AXIAL GAS TEMPERATURE PROFILES

FEED MIXTURE RATIO = 4.0 LB O_2/LB H_2 (4.0 KG O_2 /KG H_2)

NOMINAL CHAMBER PRESSURE = 300 PSIA (2.07×10^6 N/M^2)

FEED TEMPERATURE = 360 DEG R (200 DEG K)

INITIAL BED TEMPERATURE = 360 DEG R (200 DEG K)

MASS FLOW RATE = 1.05 LB/FT^2-SEC (5.13 KG/M^2 - SEC)

CATALYST PARTICLE SIZE = 14-18 MESH

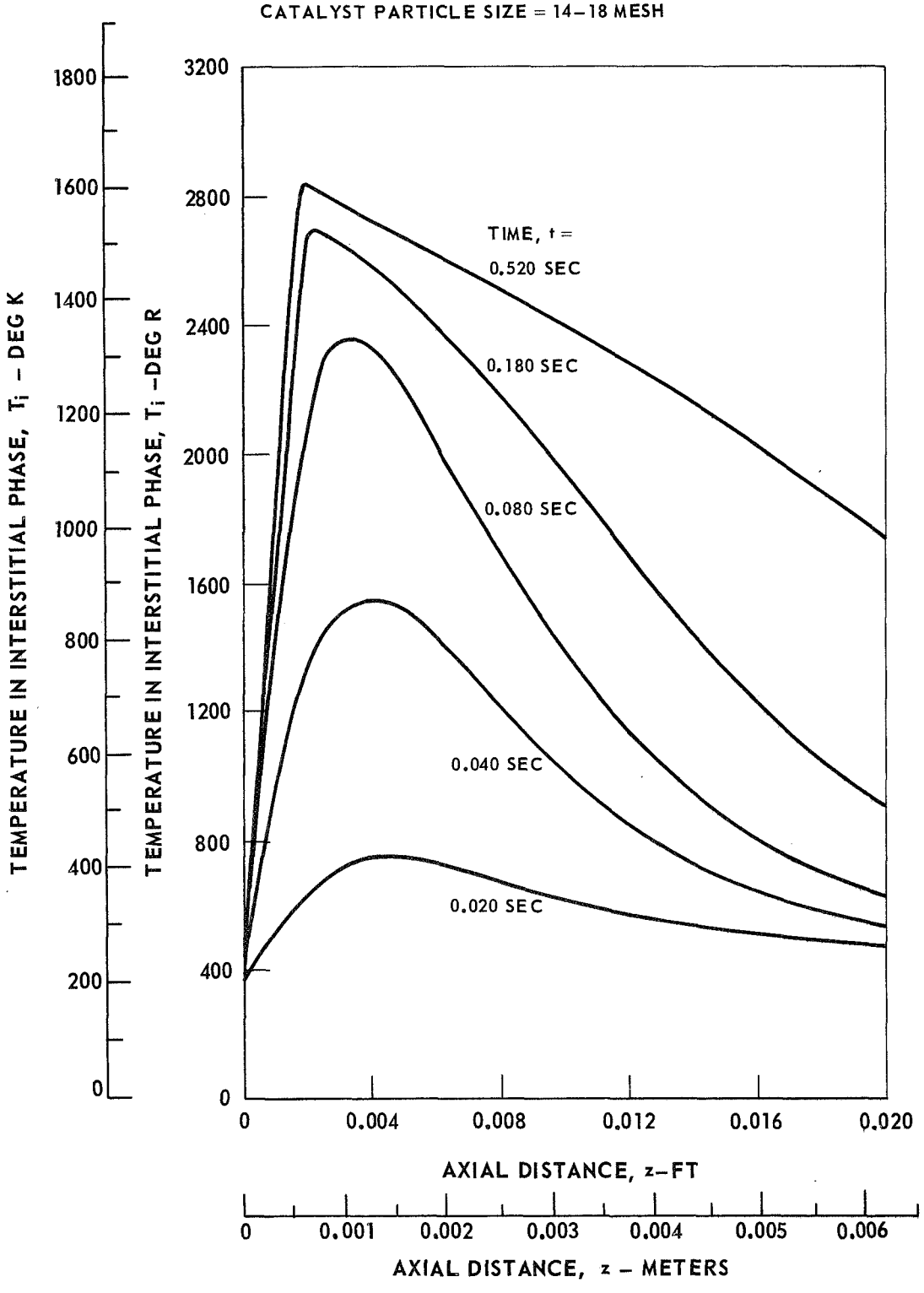

VARIATION OF EXIT GAS TEMPERATURE WITH TIME FOR VARIOUS FEED MIXTURE RATIOS

NOMINAL CHAMBER PRESSURE = 300 PSIA (2.07×10^6 N/M^2)

FEED TEMPERATURE = 360 DEG R (200 DEG K)

INITIAL BED TEMPERATURE = 360 DEG R (200 DEG K)

MASS FLOW RATE = 1.05 LB/FT^2-SEC (5.13 KG/M^2 - SEC)

CATALYST PARTICLE SIZE = 14-18 MESH

LINES	FUEL MIXTURE RATIO (LB O_2/LB H_2) (KG O_2/KG H_2)
——— - ———	1.0
— — — — —	2.0
———————	4.0

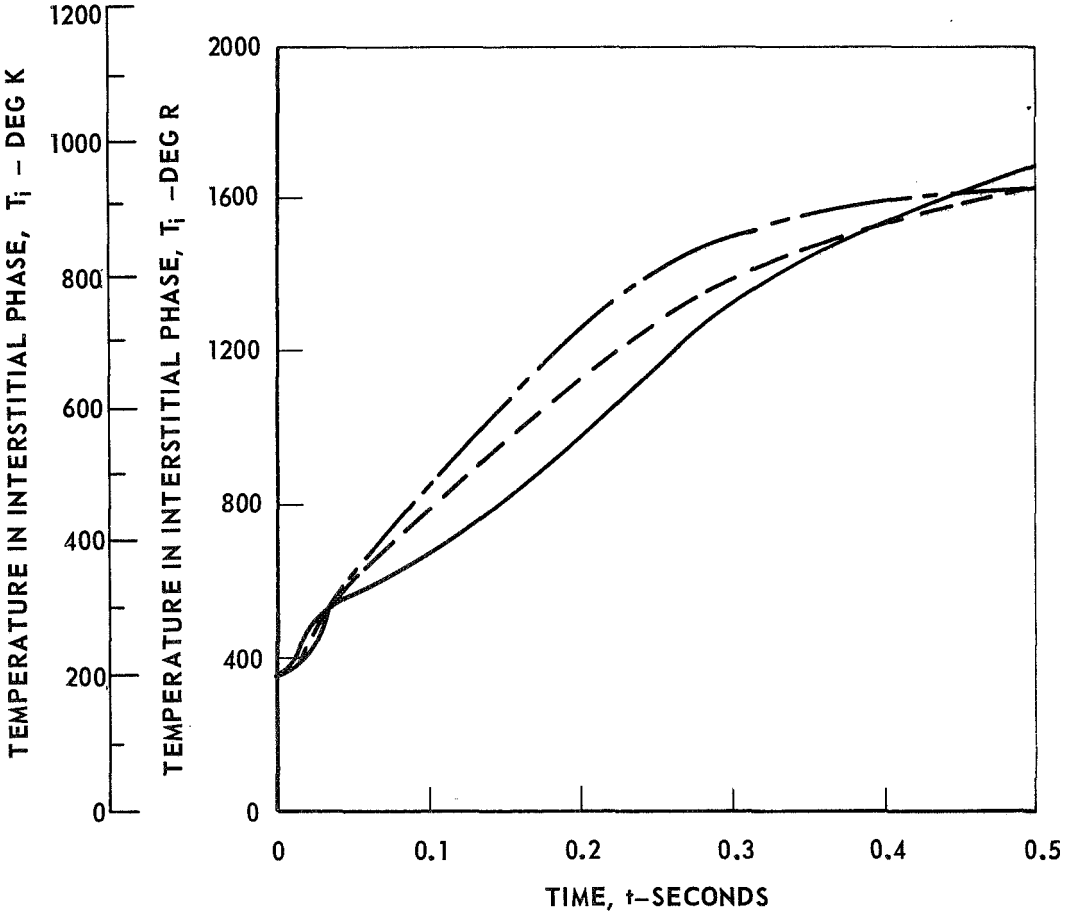

VARIATION OF MID-BED GAS TEMPERATURE WITH TIME FOR VARIOUS FEED MIXTURE RATIOS

NOMINAL CHAMBER PRESSURE = 300 PSIA (2.07×10^6 N/M^2)

FEED TEMPERATURE = 360 DEG R (200 DEG R)

INITIAL BED TEMPERATURE = 360 DEG R (200 DEG R)

MASS FLOW RATE = 1.05 LB/FT^2-SEC (5.13 KG/M^2 - SEC)

CATALYST PARTICLE SIZE = 14-18 MESH

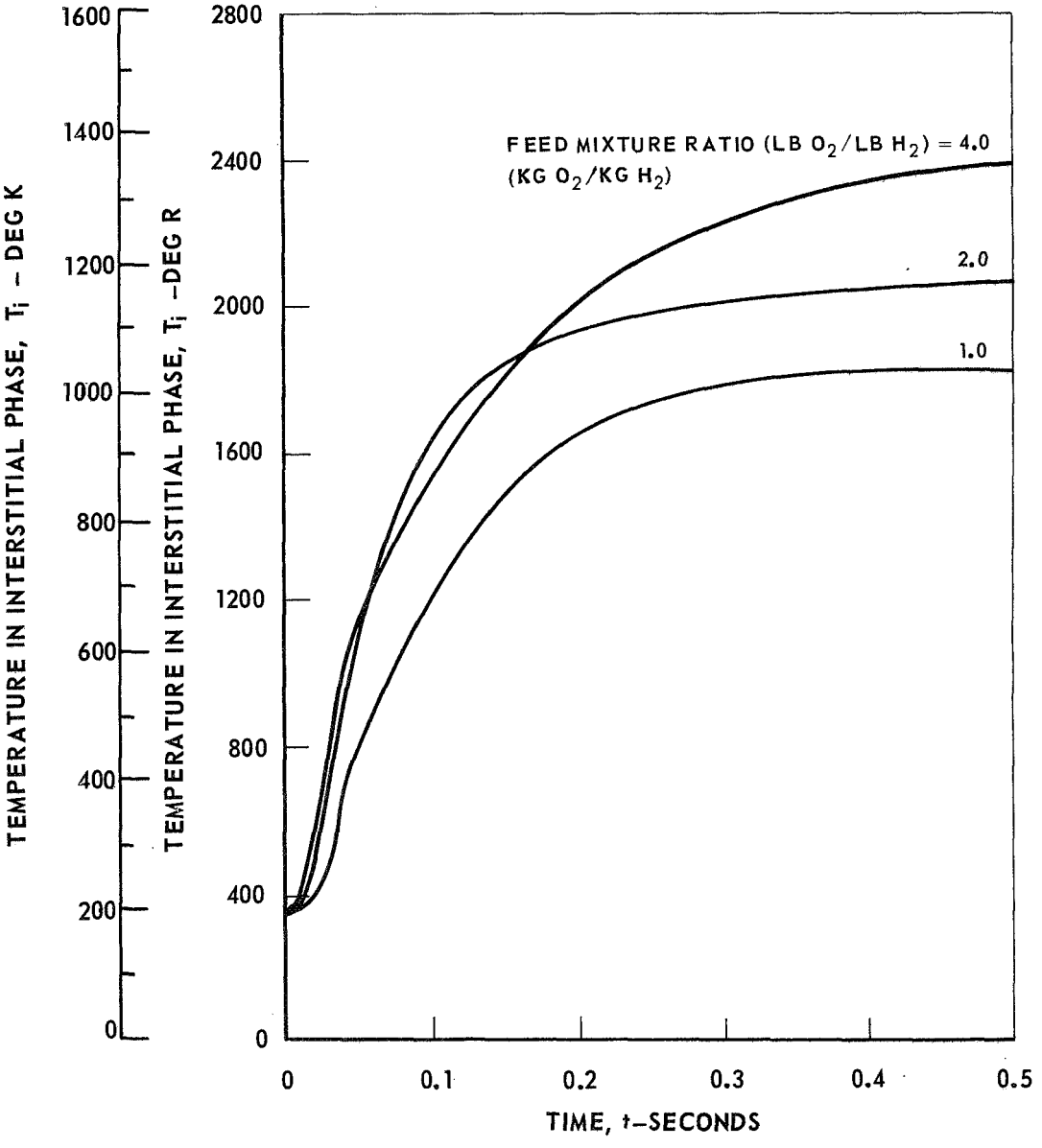

TRANSIENT AXIAL GAS TEMPERATURE PROFILES

FEED TEMPERATURE = 530 DEG R (295 DEG K)

INITIAL BED TEMPERATURE = 530 DEG R (295 DEG K)

NOMINAL CHAMBER PRESSURE = 300 PSIA (2.07×10^6 N/M^2)

FEED MIXTURE RATIO = 1.0 LB O_2/LB H_2 (1.0 KG O_2/KG H_2)

MASS FLOW RATE = 1.05 LB/FT^2-SEC (5.13 KG/M^2 - SEC)

CATALYST PARTICLE SIZE = 14-18 MESH

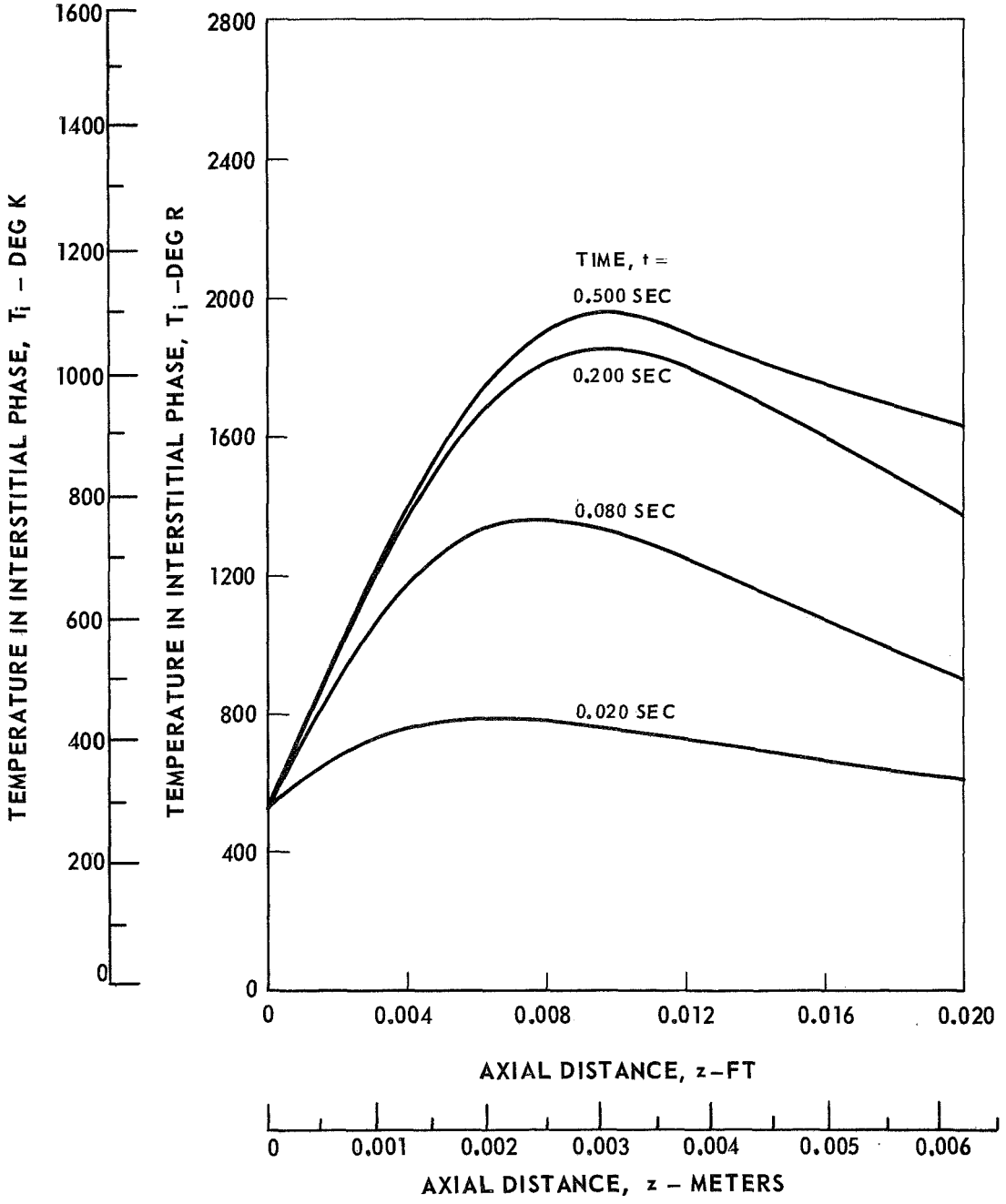

TRANSIENT AXIAL GAS TEMPERATURE PROFILES

FEED TEMPERATURE = 420 DEG R (233 DEG R)
INITIAL BED TEMPERATURE = 420 DEG R (233 DEG R)

NOMINAL CHAMBER PRESSURE = 300 PSIA (2.07×10^6 N/M^2)
FEED MIXTURE RATIO = 1.0 LB O_2/LB H_2 (1.0 KG O_2/KG H_2)
MASS FLOW RATE = 1.05 LB/FT^2-SEC (5.13 KG/M^2 - SEC)
CATALYST PARTICLE SIZE = 14-18 MESH

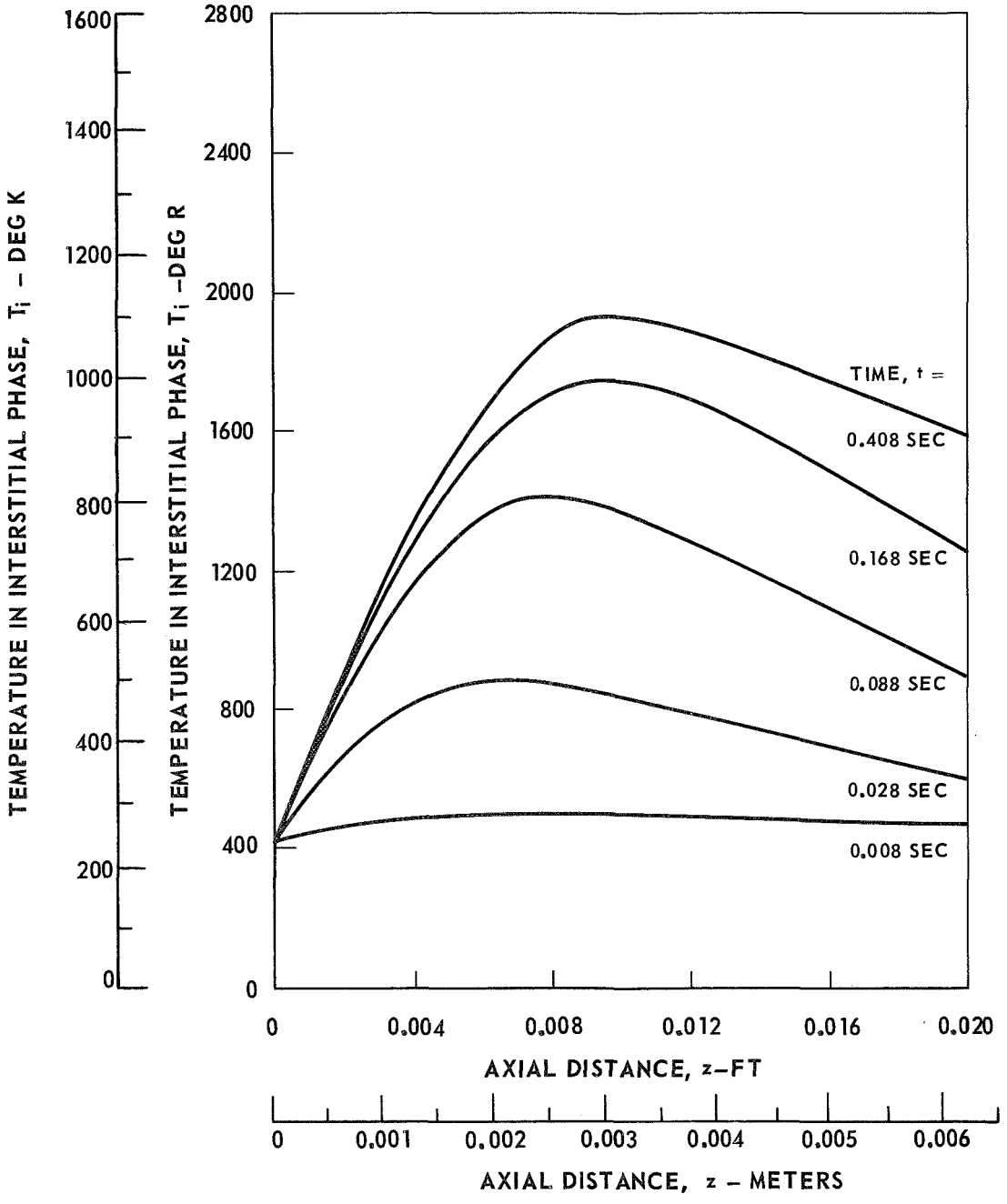

TRANSIENT AXIAL GAS TEMPERATURE PROFILES

FEED TEMPERATURE = 330 DEG R (183 DEG K)

INITIAL BED TEMPERATURE = 330 DEG R (183 DEG K)

NOMINAL CHAMBER PRESSURE = 300 PSIA (2.07×10^6 N/M^2)

FEED MIXTURE RATIO = 1.0 LB O_2/LB H_2 (1.0 KG O_2/KG H_2)

MASS FLOW RATE = 1.05 LB/FT^2-SEC (5.13 KG/M^2 - SEC)

CATALYST PARTICLE SIZE = 14-18 MESH

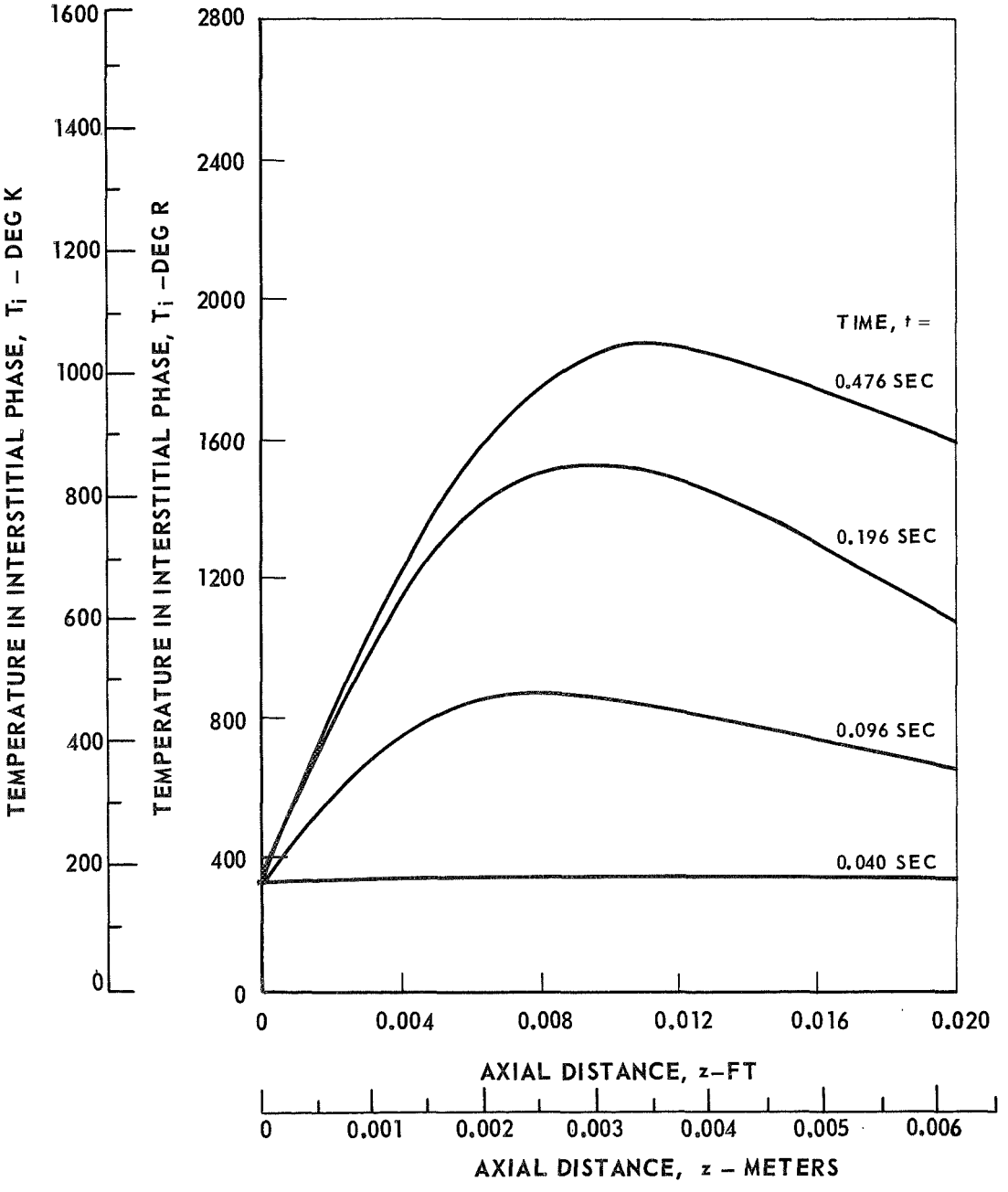

TRANSIENT AXIAL GAS TEMPERATURE PROFILES

FEED TEMPERATURE = 300 DEG R (167 DEG K)
INITIAL BED TEMPERATURE = 300 DEG R (167 DEG K)

NOMINAL CHAMBER PRESSURE = 300 PSIA (2.07×10^6 N/M^2)
FEED MIXTURE RATIO = 1.0 LB O_2/LB H_2 (1.0 KG O_2/KG H_2)
MASSFLOW RATE = 1.05 LB/FT^2-SEC (5.13 KG/M^2 - SEC)
CATALYST PARTICLE SIZE = 14-18 MESH

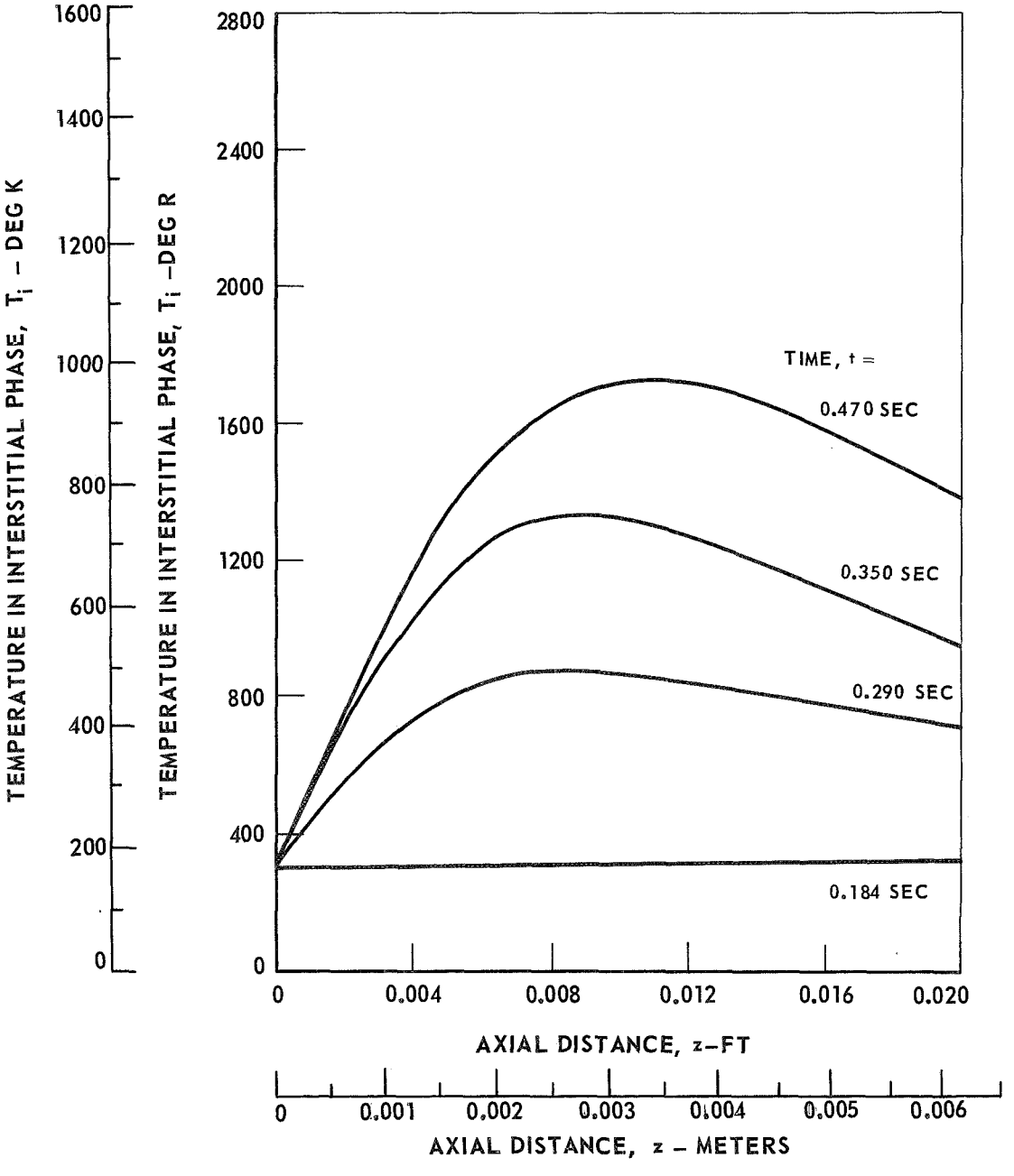

VARIATION OF EXIT GAS TEMPERATURE WITH TIME FOR VARIOUS FEED TEMPERATURES

NOMINAL CHAMBER PRESSURE = 300 PSIA (2.07×10^6 N/M^2)

INITIAL BED TEMPERATURES = FEED TEMPERATURES

FEED MIXTURE RATIO = 1.0 LB O_2/LB H_2 (1.0 KG O_2/KG H_2)

MASS FLOW RATE = 1.05 LB/FT^2-SEC (5.13 KG/M^2 - SEC)

CATALYST PARTICLE SIZE = 14-18 MESH

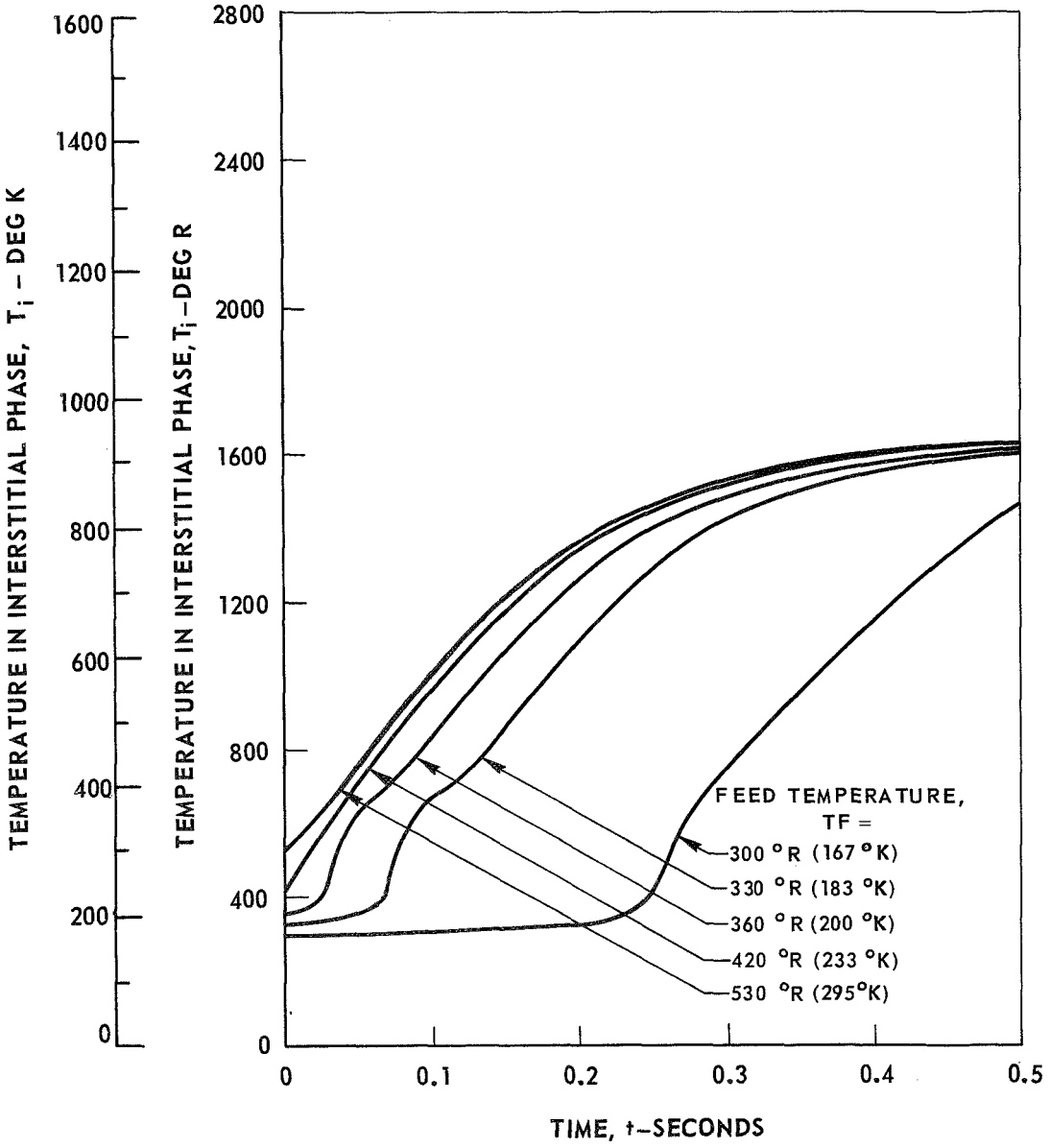

TRANSIENT AXIAL GAS TEMPERATURE PROFILES

INITIAL BED TEMPERATURE = 530 DEG R (295 DEG K)

NOMINAL CHAMBER PRESSURE = 300 PSIA (2.07×10^6 KG/M^2)

FEED TEMPERATURE = 360 DEG R (200 DEG K)

FEED MIXTURE RATIO = 1.0 LB O_2/LB H_2 (1.0 KG O_2 /KG H_2)

MASS FLOW RATE = 1.05 LB/FT^2 -SEC (5.13 KG/M^2 - SEC)

CATALYST PARTICLE SIZE = 14-18 MESH

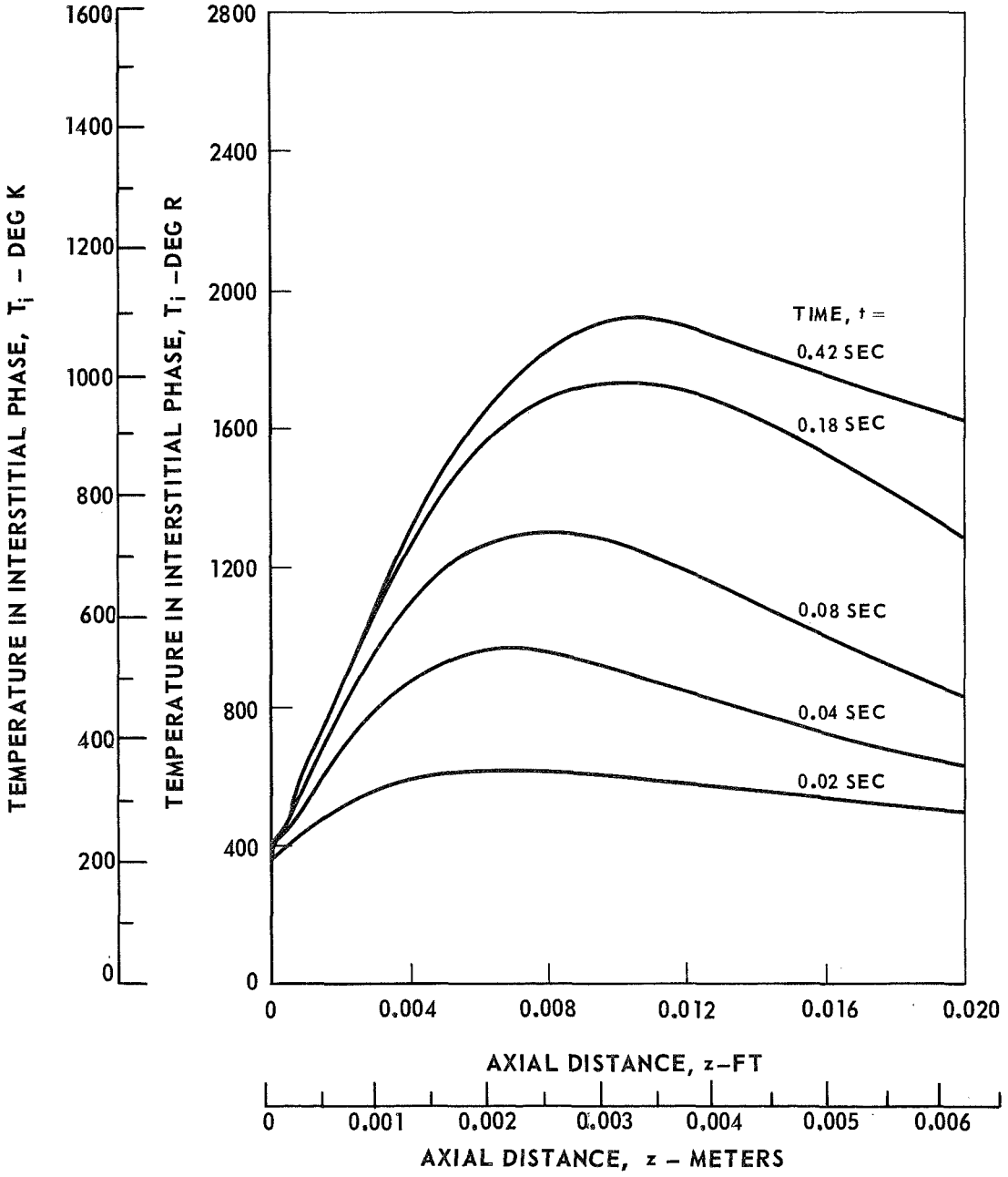

VARIATION OF EXIT GAS TEMPERATURE WITH TIME FOR TWO INITIAL BED TEMPERATURES

NOMINAL CHAMBER PRESSURE = 300 PSIA (2.07×10^6 N/M^2)

FEED TEMPERATURE = 360 DEG R (200 DEG K)

FEED MIXTURE RATIO = 1.0 LB O_2/LB H_2 (1.0 KG O_2/KG H_2)

MASS FLOW RATE = 1.05 LB/FT^2-SEC (5.13 KG/M^2 - SEC)

CATALYST PARTICLE SIZE = 14-18 MESH

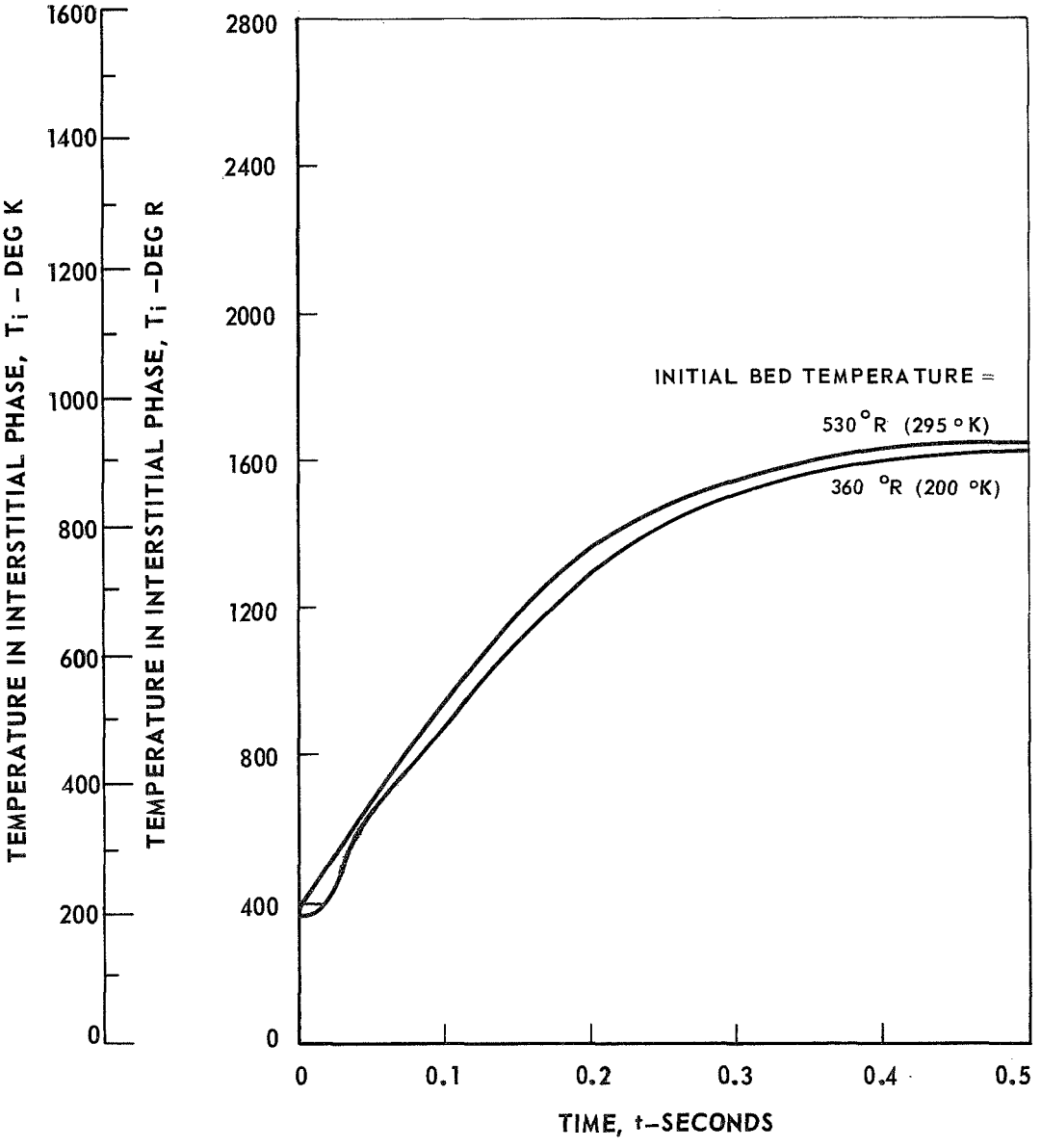

TRANSIENT AXIAL GAS TEMPERATURE PROFILES

MASS FLOW RATE = 2.10 LB/FT^2-SEC (10.26 KG/M^2 - SEC)

NOMINAL CHAMBER PRESSURE = 300 PSIA (2.07X10^6 N/M^2)

FEED TEMPERATURE = 360 DEG R (200 DEG R)

INITIAL BED TEMPERATURE = 360 DEG R (200 DEG R)

FEED MIXTURE RATIO = 1.0 LB O_2/LB H_2 (1.0 KG O_2/KG H_2)

CATALYST PARTICLE SIZE = 14-18 MESH

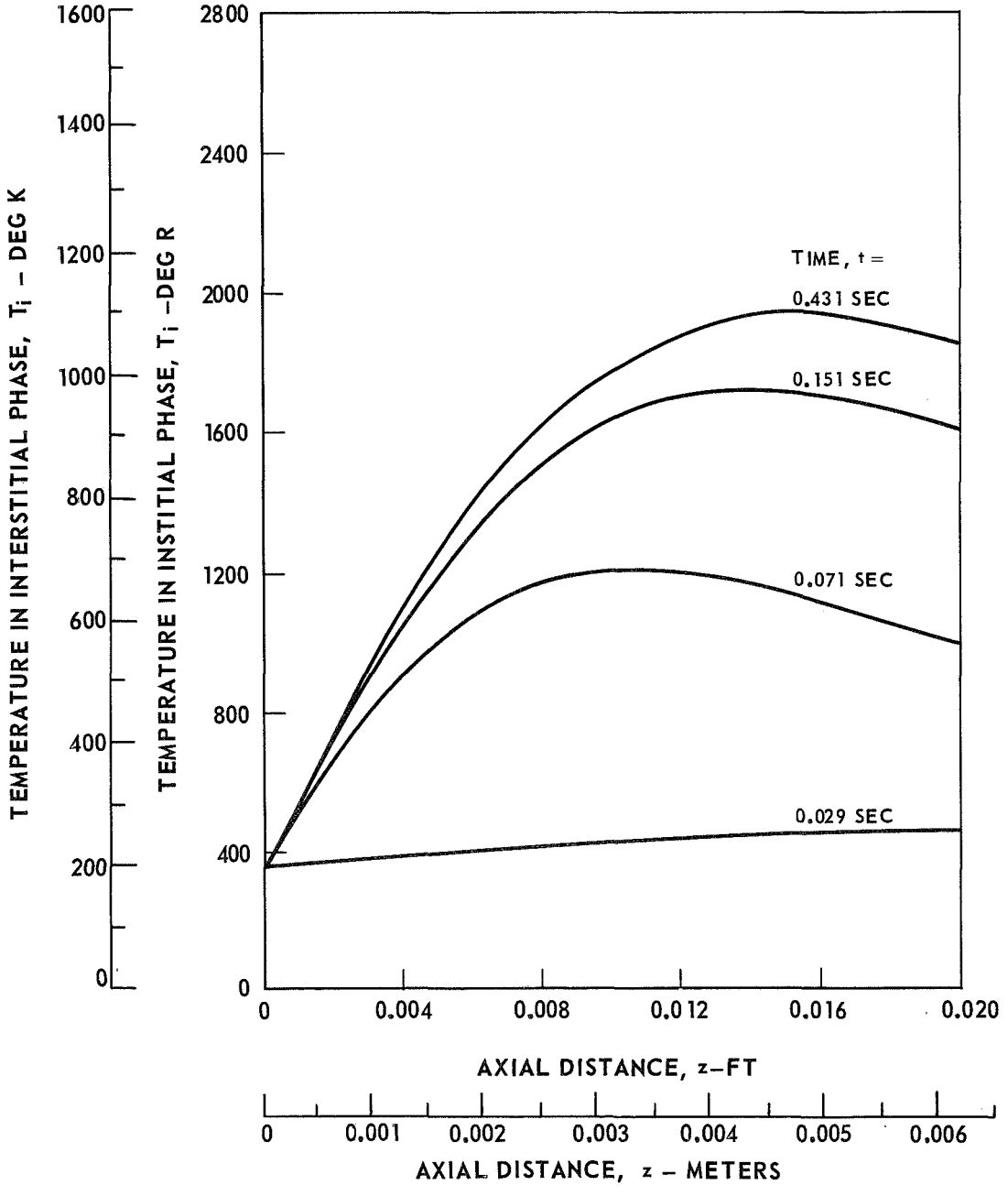

VARIATION OF EXIT GAS TEMPERATURE WITH TIME FOR TWO MASS FLOW RATES

NOMINAL CHAMBER PRESSURE = 300 PSIA (2.07×10^6 N/M^2)

FEED TEMPERATURE = 360 DEG R (200 DEG K)

INITIAL BED TEMPERATURE = 360 DEG R (200 DEG K)

FEED MIXTURE RATIO = 1.0 LB O_2/LB H_2 (1.0 KG O_2/KG H_2)

CATALYST PARTICLE SIZE = 14-18 MESH

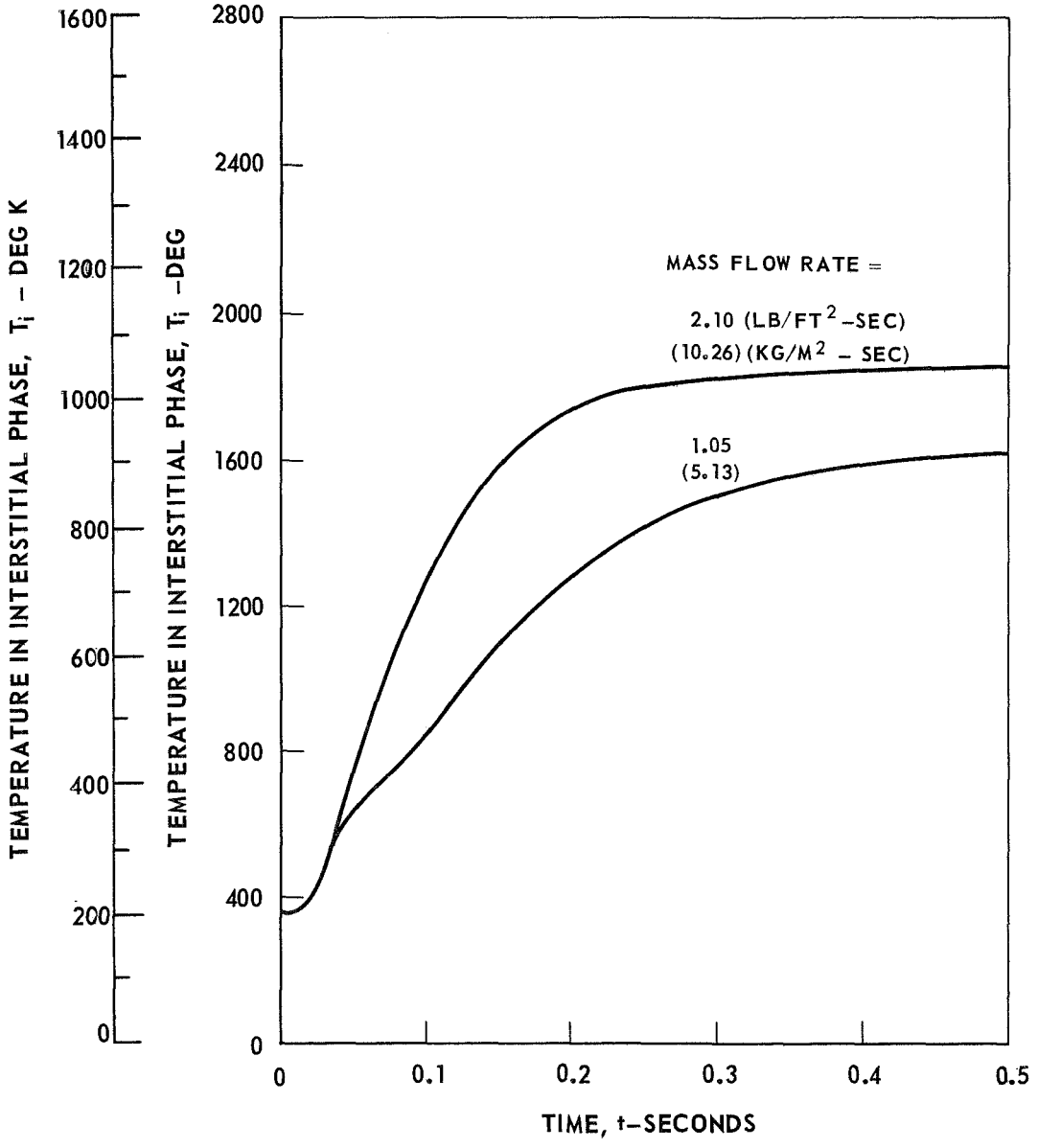

TRANSIENT AXIAL GAS TEMPERATURE PROFILES

CATALYST PARTICLE SIZE = 25-30 MESH

NOMINAL CHAMBER PRESSURE = 300 PSIA (2.07×10^6 N/M^2)

FEED TEMPERATURE = 360 DEG R (200 DEG K)

INITIAL BED TEMPERATURE = 360 DEG R (200 DEG K)

FEED MIXTURE RATIO = 1.0 LB O_2/LB H_2 (1.0 KG O_2/KG H_2)

MASS FLOW RATE = 1.05 LB/FT^2-SEC (5.13 KG/M^2 - SEC)

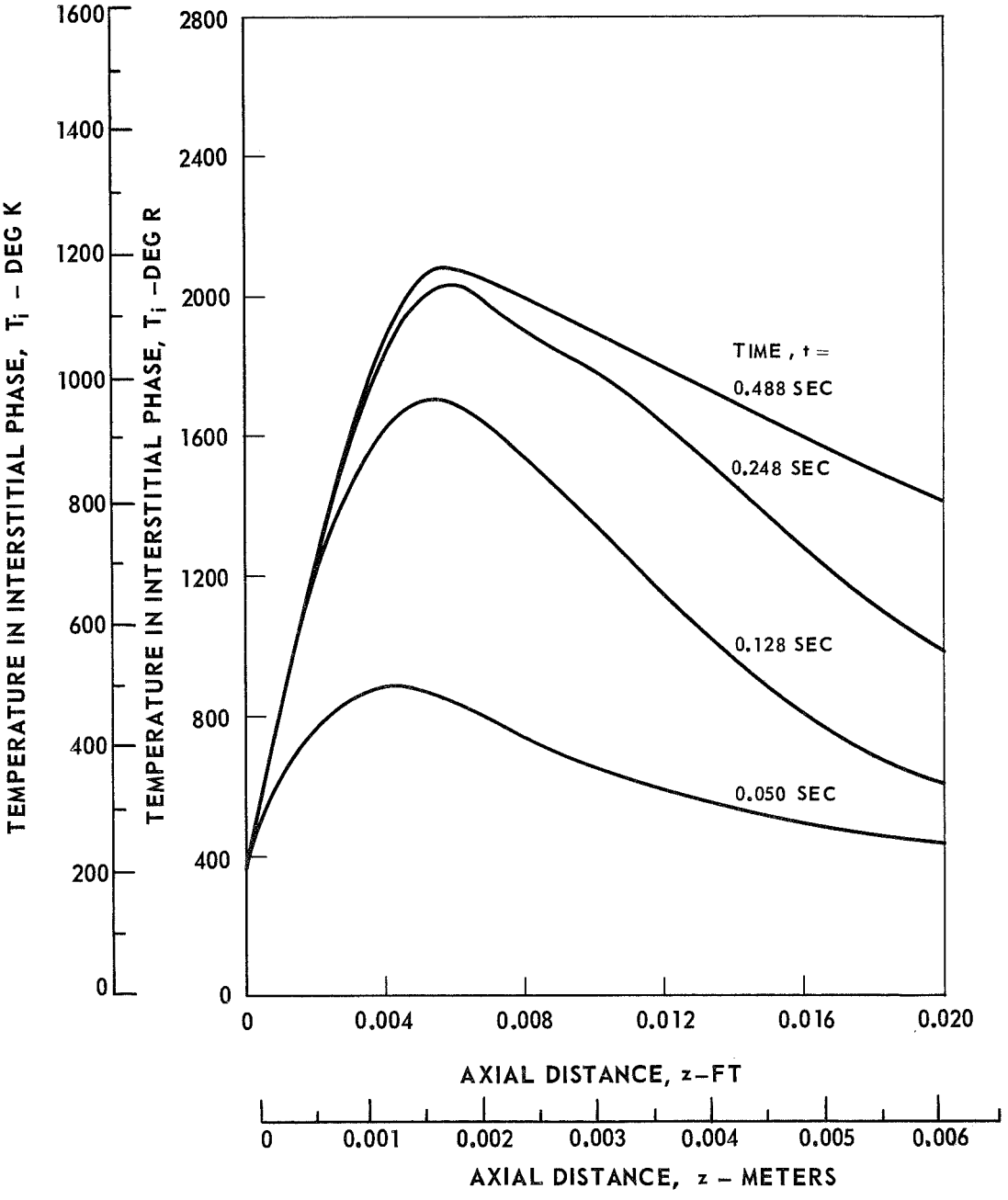

VARIATION OF GAS TEMPERATURE WITH TIME AT TWO AXIAL POSITIONS FOR TWO CATALYST PARTICLE SIZES

NOMINAL CHAMBER PRESSURE = 300 PSIA (2.07×10^6 N/M^2)
FEED TEMPERATURE = 360 DEG R (200 DEG K)
INITIAL BED TEMPERATURE = 360 DEG R (200 DEG K)
FEED MIXTURE RATIO = 1.0 LB O_2/LB H_2 (1.0 KG O_2/KG H_2)
MASS FLOW RATE = 1.05 LB/FT^2-SEC (5.13 KG/M^2 - SEC)

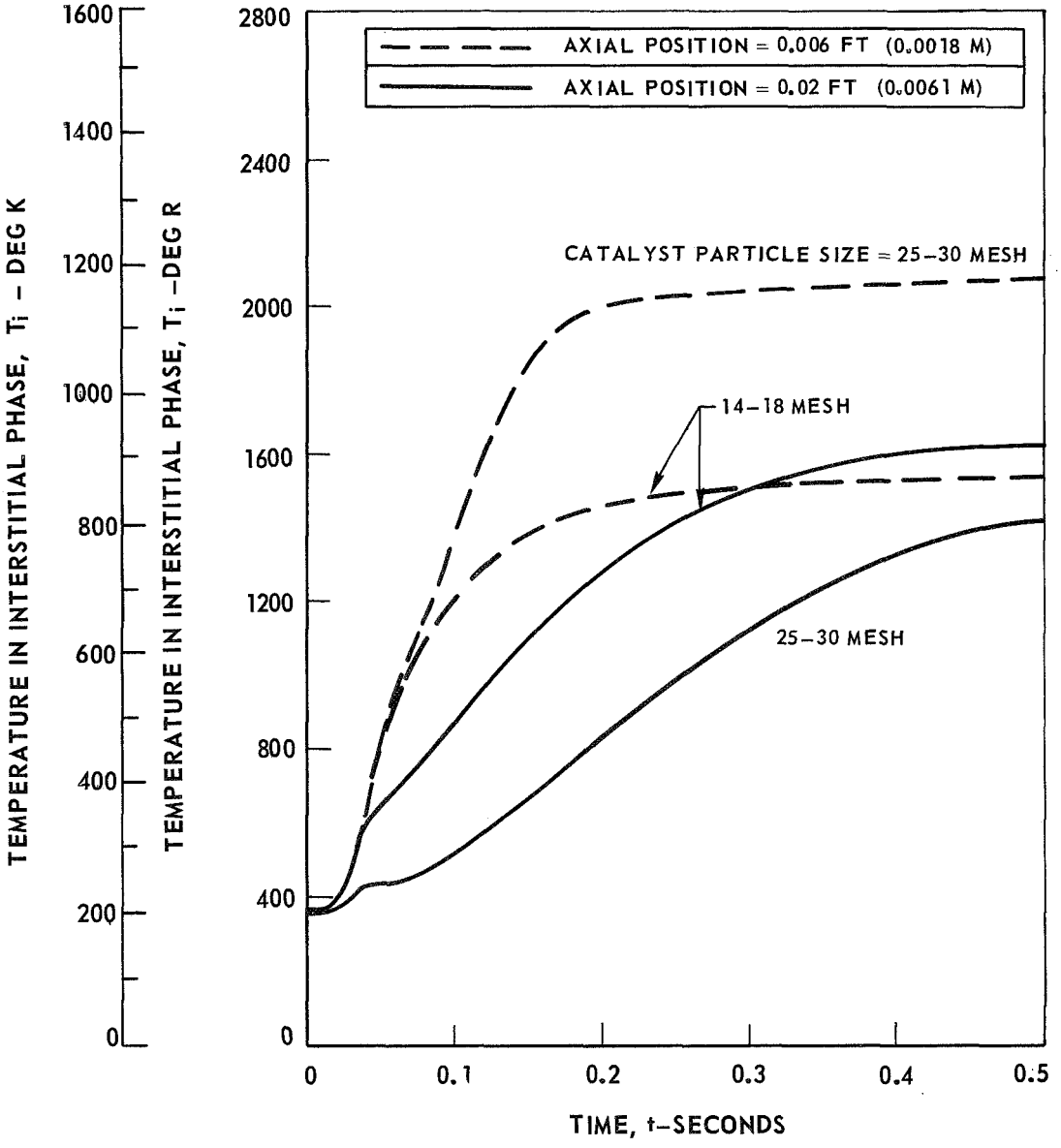

TRANSIENT AXIAL GAS TEMPERATURE PROFILES

NOMINAL CHAMBER PRESSURE = 15 PSIA (1.04 X 10^5 N/M^2)

FEED TEMPERATURE = 360 DEG R (200 DEG K)

INITIAL BED TEMPERATURE = 360 DEG R (200 DEG K)

FEED MIXTURE RATIO = 1.0 LB O_2/LB H_2 (1.0 KG O_2/KG H_2)

MASS FLOW RATE = 0.26 LB/FT^2-SEC (1.25 KG/M^2-SEC)

CATALYST PARTICLE SIZE = 14-18 MESH

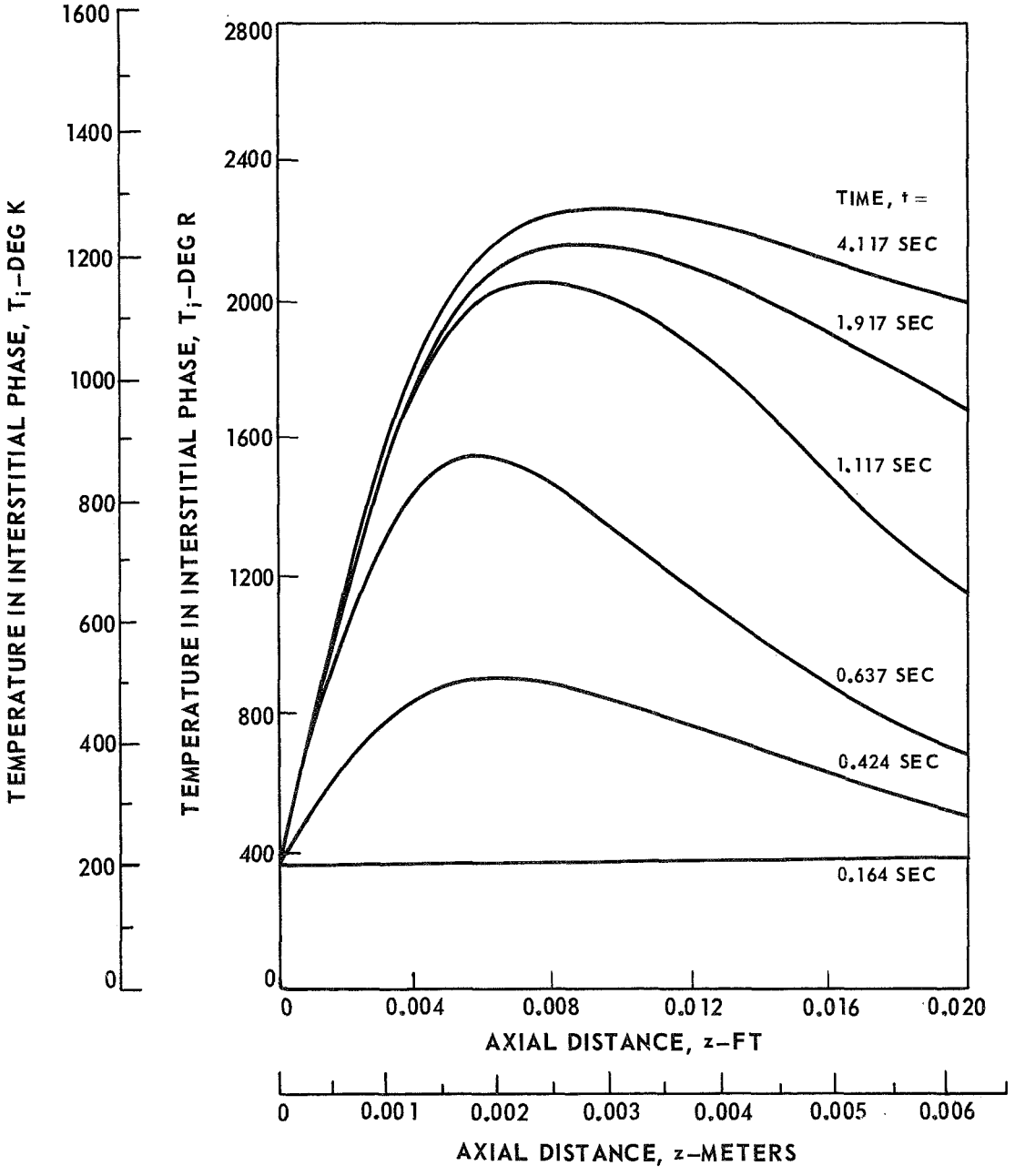

TRANSIENT AXIAL PROFILES OF PARTICLE SURFACE TEMPERATURES

NOMINAL CHAMBER PRESSURE = 15 PSIA (1.04×10^5 N/M^2)

FEED TEMPERATURE = 360 DEG R (200 DEG K)

INITIAL BED TEMPERATURE = 360 DEG R (200 DEG K)

FEED MIXTURE RATIO = 1.0 LB O_2/LB H_2 (1.0 KG O_2/KG H_2)

MASS FLOW RATE = 0.26 LB/FT^2-SEC (1.25 KG/M^2-SEC)

CATALYST PARTICLE SIZE = 14-18 MESH

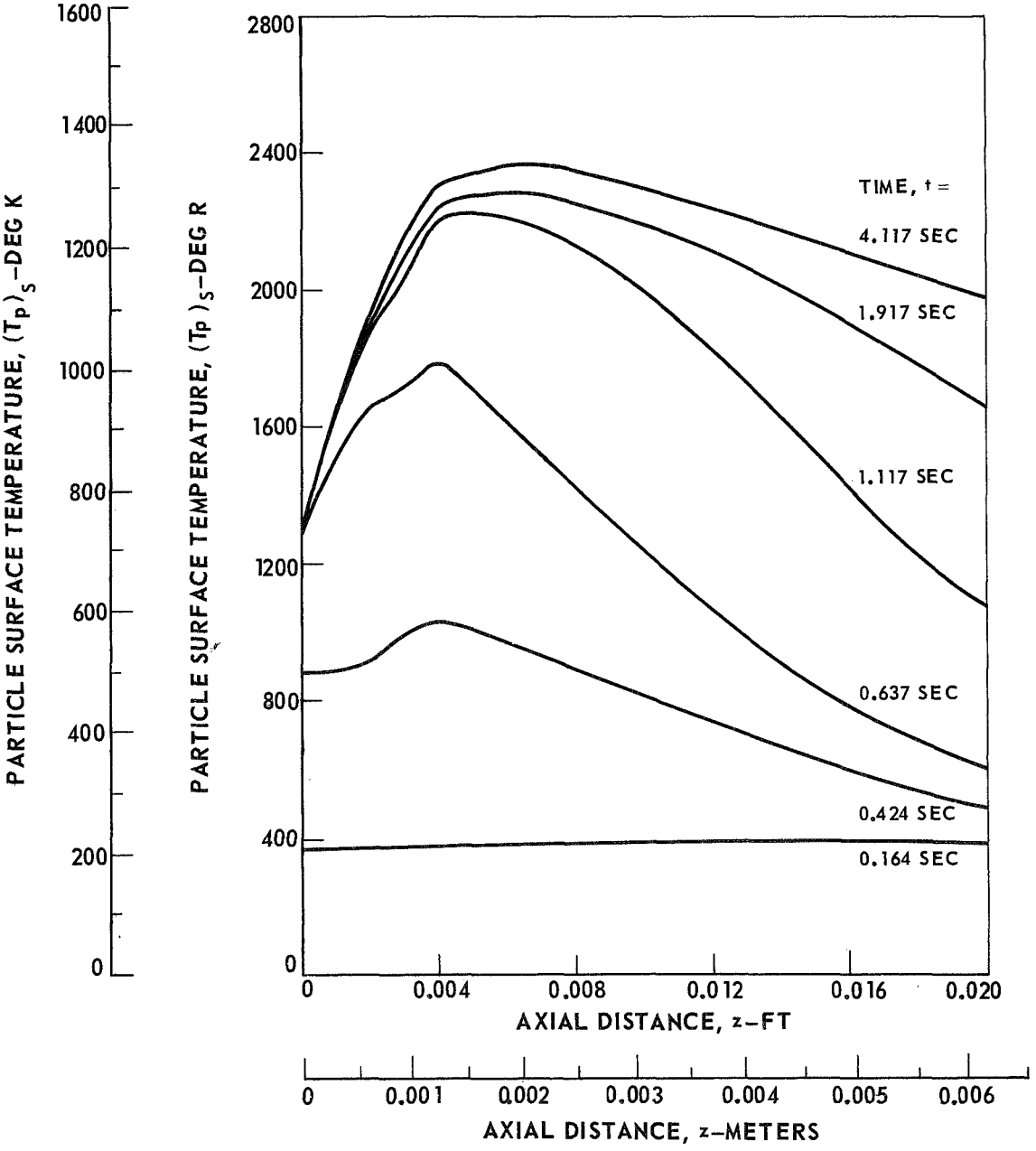

VARIATIONS OF GAS, PARTICLE SURFACE, AND WALL TEMPERATURES WITH TIME AT TWO AXIAL POSITIONS

NOMINAL CHAMBER PRESSURE = 15 PSIA (1.04×10^5 N/M^2)
FEED TEMPERATURE = 360 DEG R (200 DEG K)
INITIAL BED TEMPERATURE = 360 DEG R (200 DEG K)
FEED MIXTURE RATIO = 1.0 LB O_2/LB H_2 (1.0 KG O_2/KG H_2)
MASS FLOW RATE = 0.26 LB/FT^2-SEC (1.25 KG/M^2-SEC)
CATALYST PARTICLE SIZE = 14-18 MESH

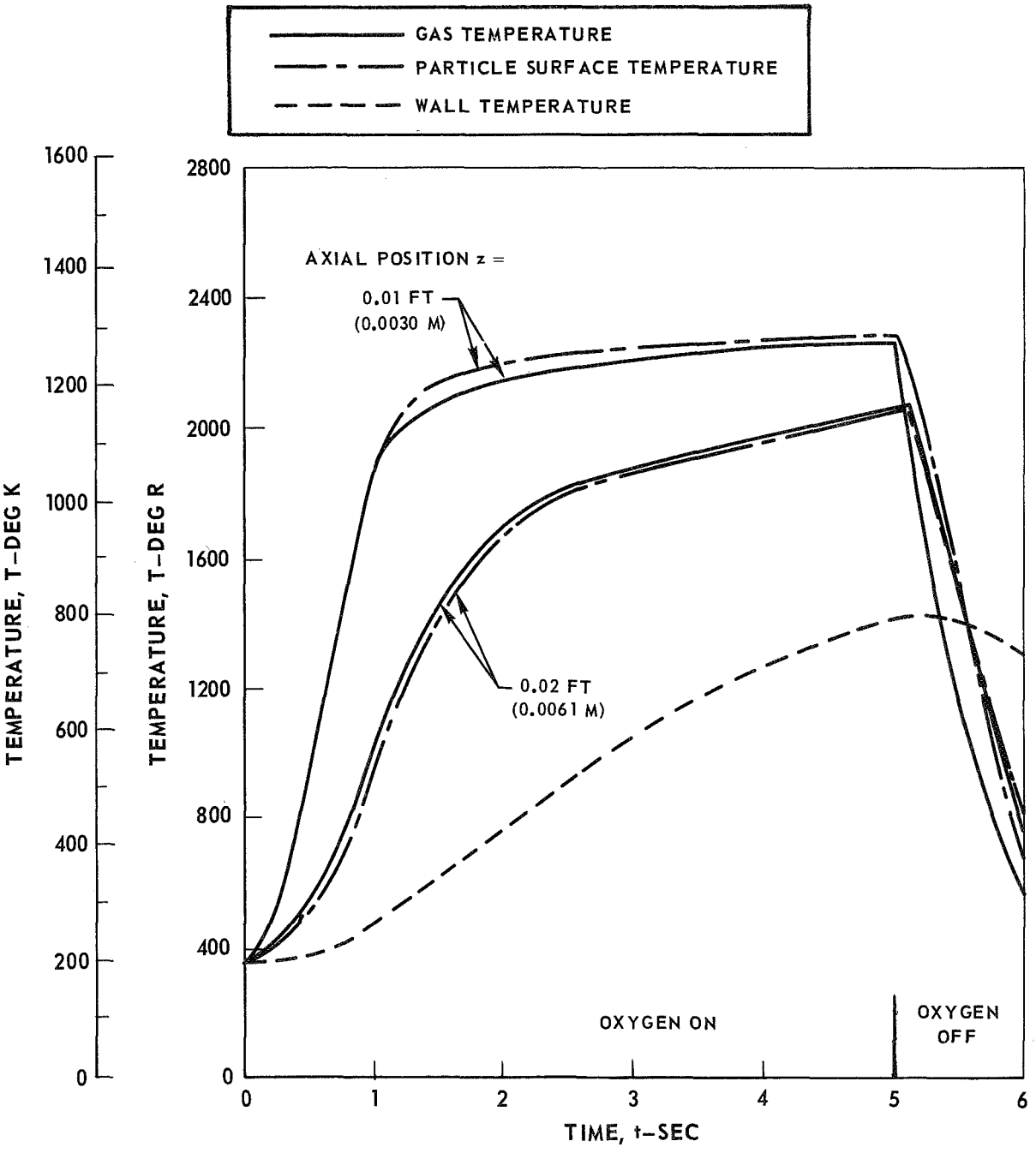

TRANSIENT AXIAL PROFILES OF MOLE-FRACTION OF OXYGEN IN GAS PHASE

NOMINAL CHAMBER PRESSURE = 15 PSIA (1.04×10^5 N/M^2)

FEED TEMPERATURE = 360 DEG R (200 DEG K)

INITIAL BED TEMPERATURE = 360 DEG R (200 DEG K)

FEED MIXTURE RATIO = 1.0 LB O_2/LB H_2 (1.0 KG O_2/KG H_2)

MASS FLOW RATE = 0.26 LB/FT^2-SEC (1.25 KG/M^2-SEC)

CATALYST PARTICLE SIZE = 14-18 MESH

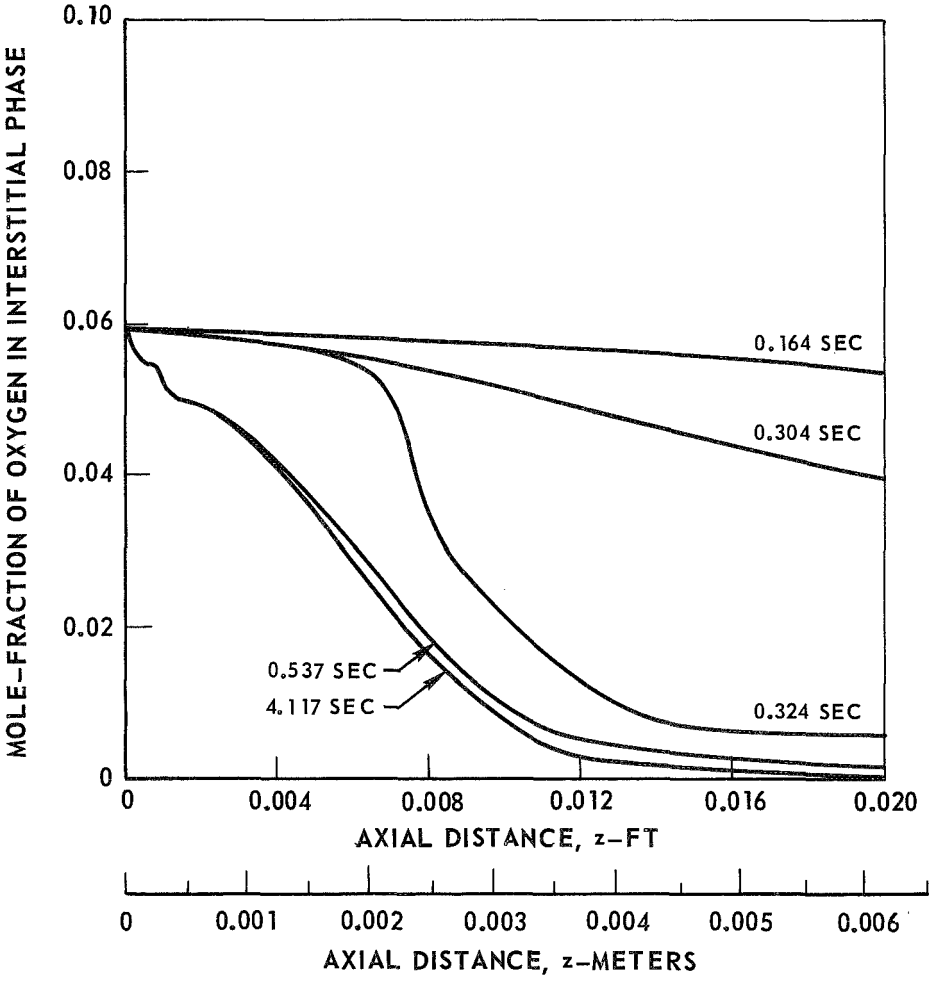

FIG. 24

TRANSIENT AXIAL GAS TEMPERATURE PROFILES

FEED MIXTURE RATIO = 4.0 LB O_2/LB H_2 (4.0 KG O_2/KG H_2)

NOMINAL CHAMBER PRESSURE = 15 PSIA (1.04 X 10^5 N/M^2)

FEED TEMPERATURE = 360 DEG R (200 DEG K)

INITIAL BED TEMPERATURE = 360 DEG R (200 DEG R)

MASS FLOW RATE = 0.26 LB/FT^2-SEC (1.25 KG/M^2-SEC)

CATALYST PARTICLE SIZE = 14-18 MESH

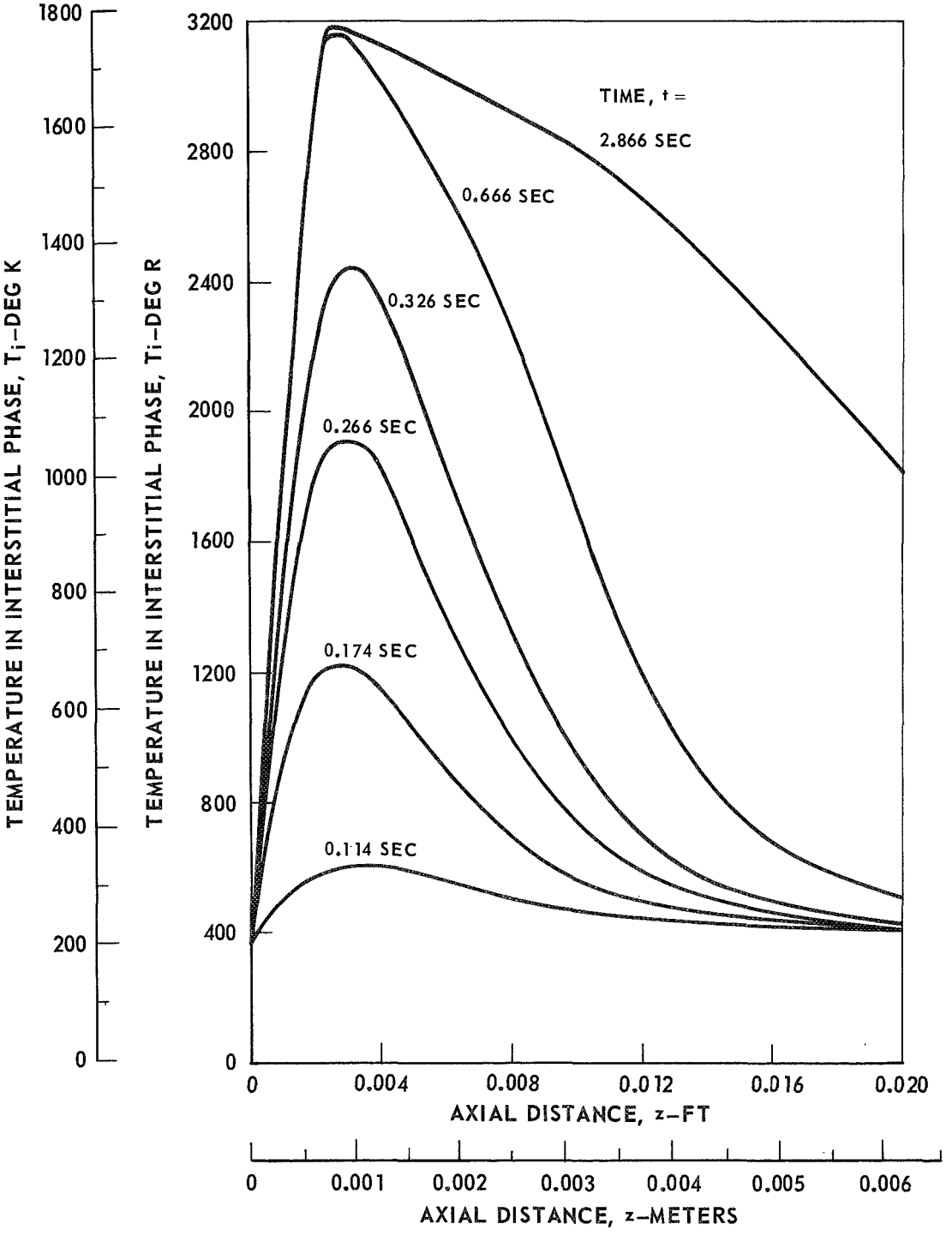

VARIATION OF EXIT GAS TEMPERATURE WITH TIME FOR TWO FEED MIXTURE RATIOS

NOMINAL CHAMBER PRESSURE = 15 PSIA (1.04×10^5 N/M^2)

FEED TEMPERATURE = 360 DEG R (200 DEG K)

INITIAL BED TEMPERATURE = 360 DEG R (200 DEG K)

MASS FLOW RATE = 0.26 LB/FT^2-SEC (1.25 KG/M^2-SEC)

CATALYST PARTICLE SIZE = 14-18 MESH

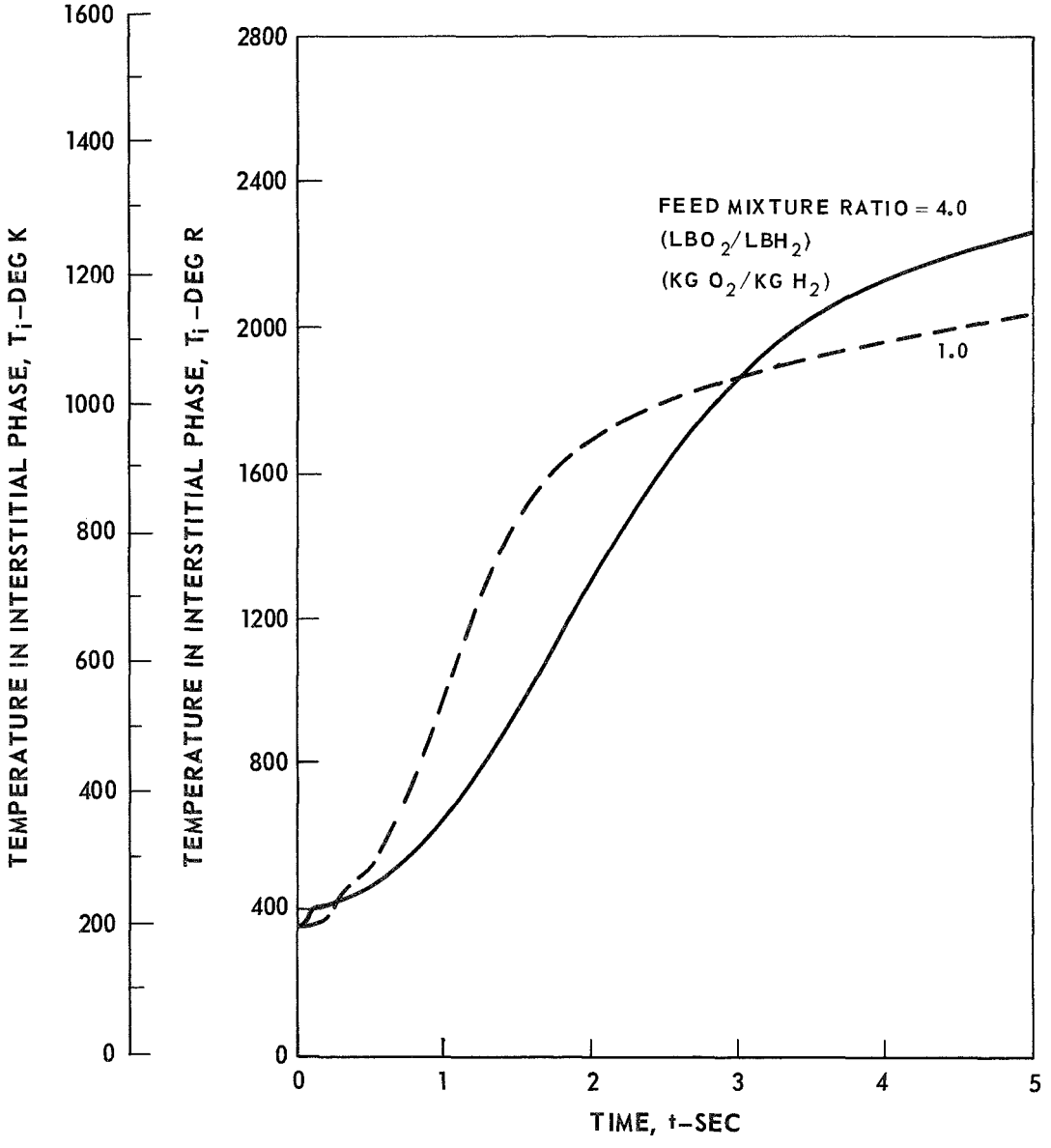

TRANSIENT AXIAL GAS TEMPERATURE PROFILES

FEED TEMPERATURE = 530 DEG R (295 DEG K)

INITIAL BED TEMPERATURE = 530 DEG R (295 DEG K)

NOMINAL CHAMBER PRESSURE = 15 PSIA (1.04×10^5 N/M^2)

FEED MIXTURE RATIO = 1.0 LBO_2/LBH_2 (1.0 KG O_2/KG H_2)

MASS FLOW RATE = 0.26 LB/FT^2-SEC (1.25 KG/M^2-SEC)

CATALYST PARTICLE SIZE = 14-18 MESH

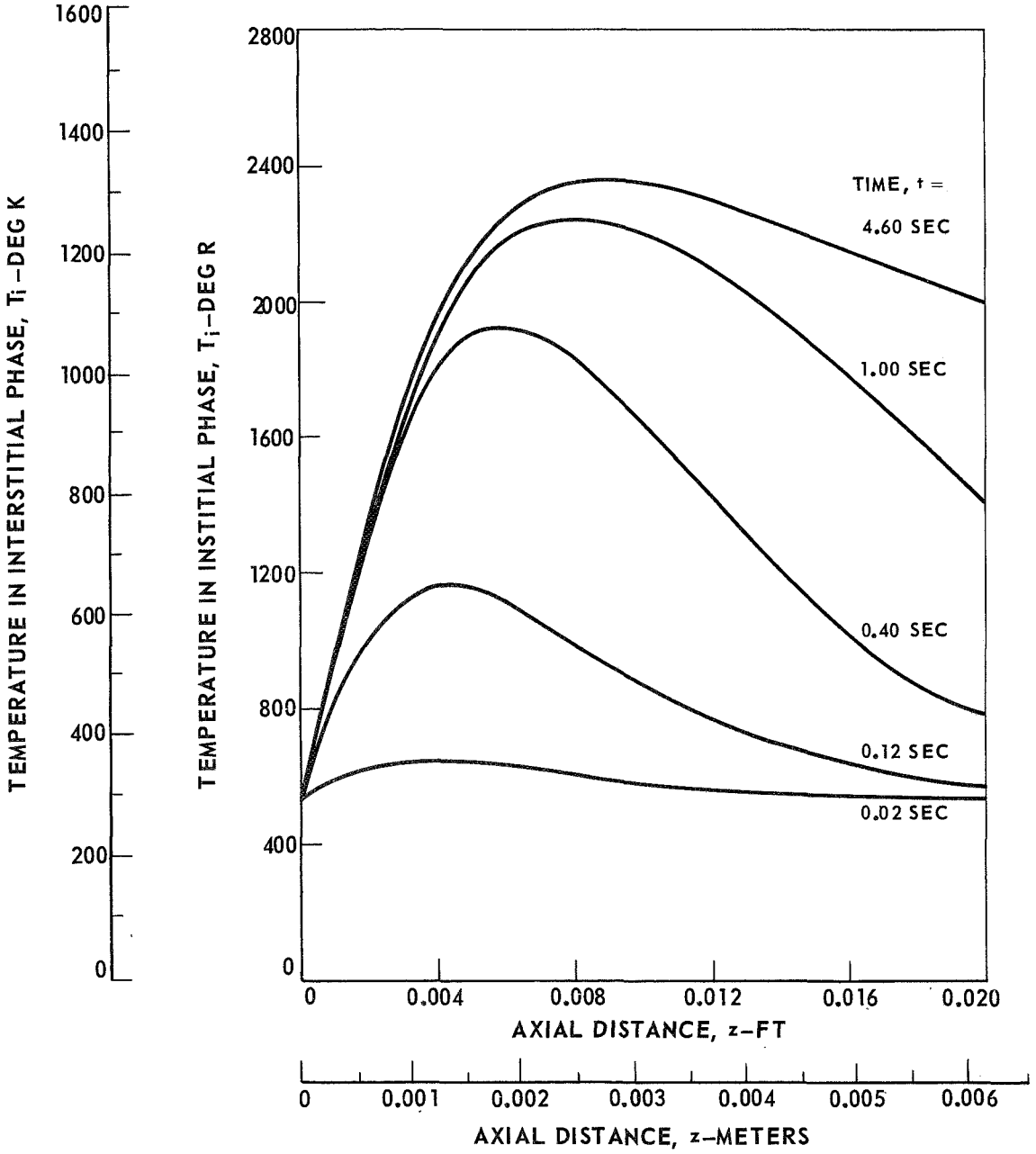

VARIATION OF EXIT GAS TEMPERATURE WITH TIME FOR TWO FEED TEMPERATURES

NOMINAL CHAMBER PRESSURE = 15 PSIA (1.04×10^5 N/M^2)

INITIAL BED TEMPERATURE = 530 & 360 DEG R 200 DEG R)

FEED MIXTURE RATIO = 1.0 LB O_2/LB H_2 (1.0 KG O_2/KG H_2)

MASS FLOW RATE = 0.26 LB/FT^2-SEC (1.25 KG/M^2-SEC)

CATALYST PARTICLE SIZE = 14-18 MESH

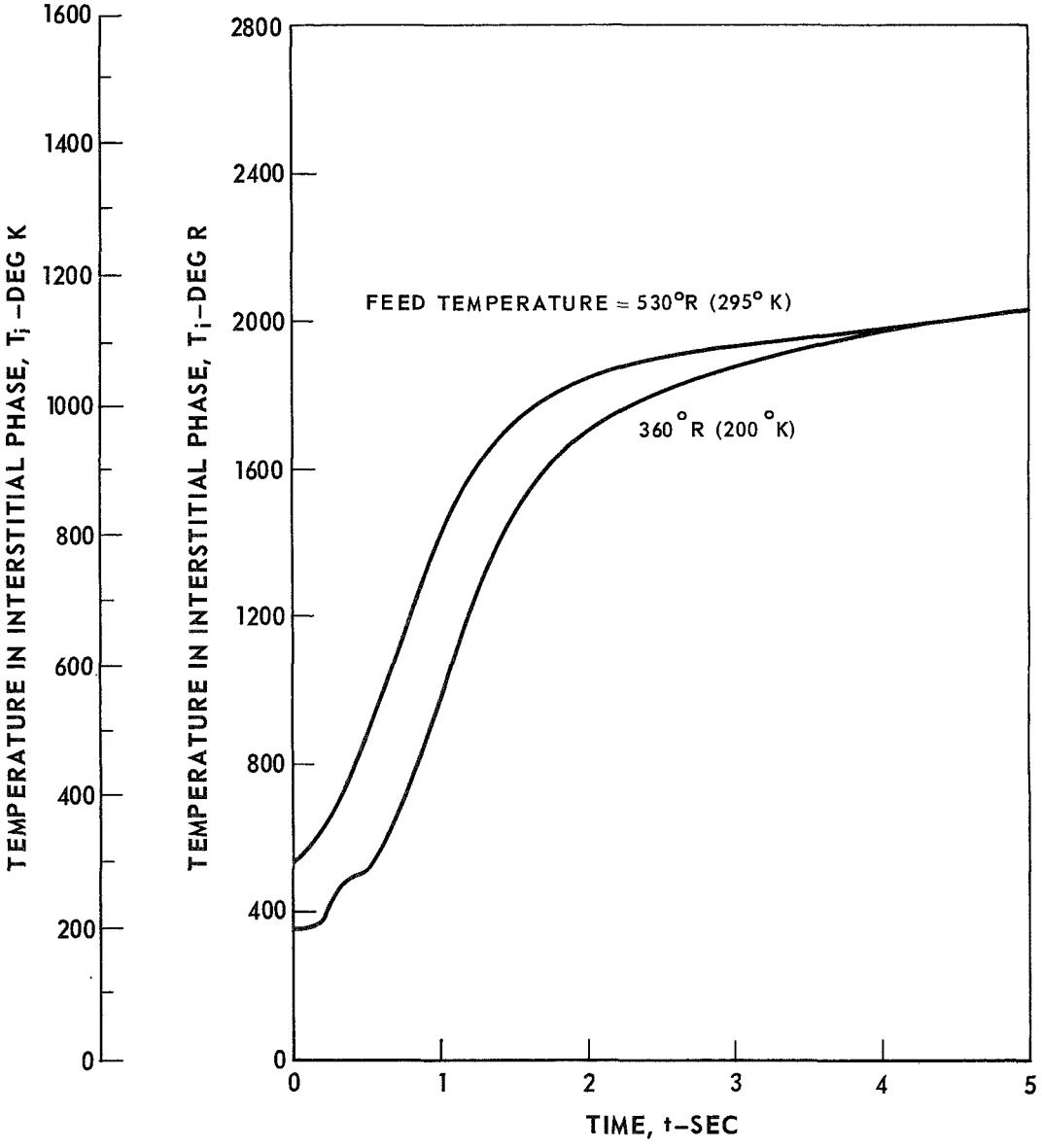

TRANSIENT AXIAL GAS TEMPERATURE PROFILES

MASS FLOW RATE = 0.51 LB/FT^2-SEC (2.50 KG/M^2-SEC)

NOMINAL CHAMBER PRESSURE = 15 PSIA (1.04 X 10^5 N/M^2)
FEED TEMPERATURE = 360 DEG R (200 DEG K)
INITIAL BED TEMPERATURE = 360 DEG R (200 DEG K)
FEED MIXTURE RATIO = 1.0 LB O_2/LB H_2 (1.0 KG O_2/KG H_2)
CATALYST PARTICLE SIZE = 14-18 MESH

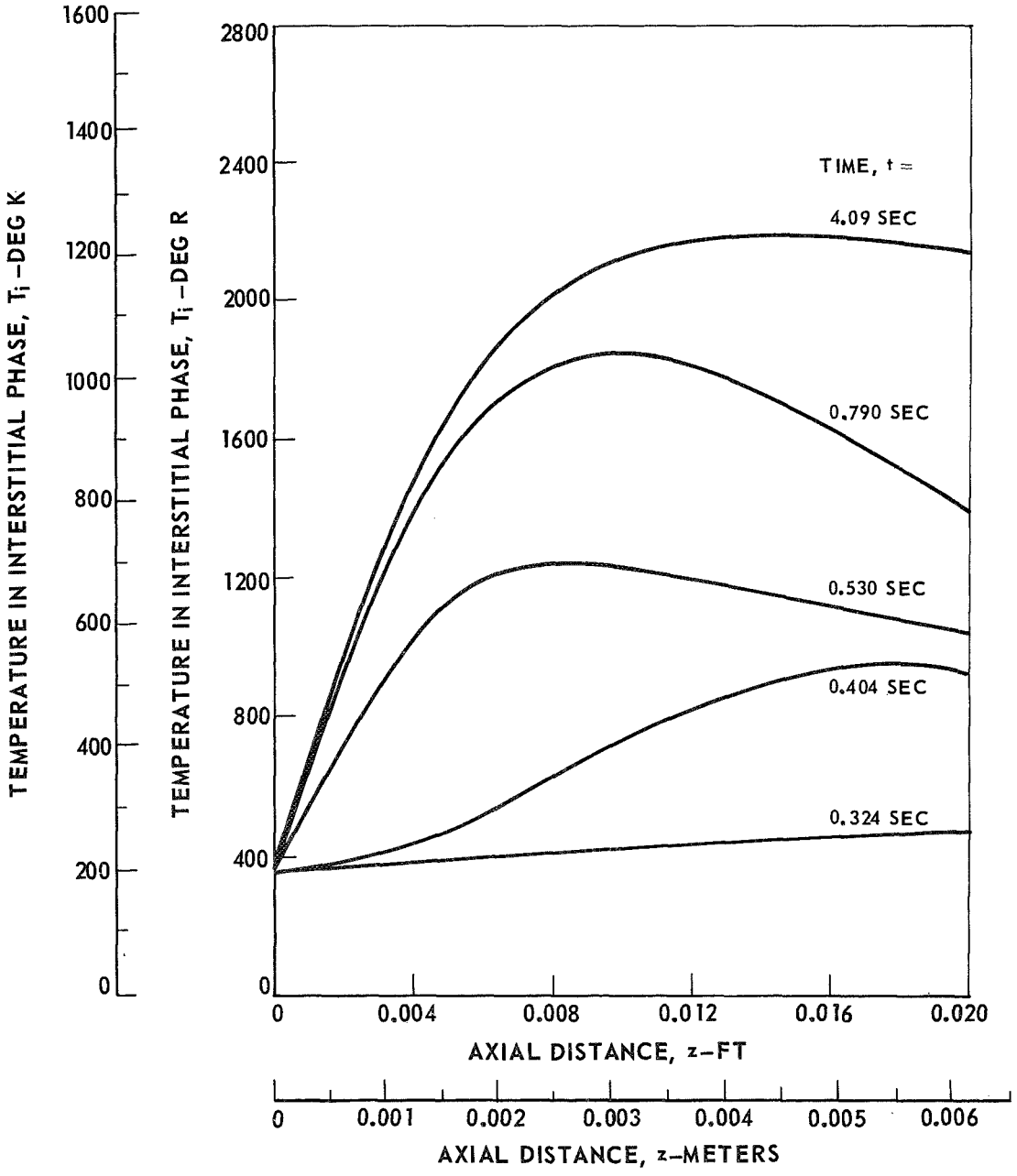

FIG. 29

VARIATION OF EXIT GAS TEMPERATURE WITH TIME FOR TWO MASS FLOW RATES

NOMINAL CHAMBER PRESSURE = 15 PSIA (1.04 X 10^5 N/M^2)

FEED TEMPERATURE = 360 DEG R (200 DEG R)

INITIAL BED TEMPERATURE = 360 DEG R (200 DEG R)

FEED MIXTURE RATIO = 1.0 LB O_2/LB H_2(1.0 KG O_2/KG H_2)

CATALYST PARTICLE SIZE = 14-18 MESH